

Transient dynamic analysis of functionally graded micro-beams considering small-scale effects

I. ESHRAGHI¹⁾, S. DAG²⁾

¹⁾*School of Engineering Science, College of Engineering, University of Tehran, P.O. Box 11155-4563, Tehran, Iran, e-mail: ieshraghi@ut.ac.ir (corresponding author)*

²⁾*Department of Mechanical Engineering, Middle East Technical University, Ankara 06800, Turkey, e-mail: sdag@metu.edu.tr*

A DOMAIN-BOUNDARY ELEMENT METHOD, based on modified couple stress theory, is developed for transient dynamic analysis of functionally graded micro-beams. Incorporating static fundamental solutions as weight functions in weighted residual expressions, governing partial differential equations of motion are converted to a set of coupled integral equations. A system of ordinary differential equations in time is obtained by domain discretization and solved using the Houbolt time marching scheme. Developed procedures are verified through comparisons to the results available in the literature for micro- and macro-scale beams. Numerical results illustrate elastodynamic responses of graded micro-beams subjected to various loading types. It is shown that metal-rich micro-beams and those with a smaller length scale parameter ratio undergo higher displacements and are subjected to larger normal stresses.

Key words: boundary element method, functionally graded materials, Timoshenko micro-beam, vibrations, modified couple stress theory.

Copyright © 2021 by IPPT PAN, Warszawa

Notation

λ, μ	Lame's constants,
ε_{ij}	strain tensor,
σ_{ij}	stress tensor,
χ_{ij}	symmetric curvature tensor,
m_{ij}	deviatoric part of the couple stress tensor,
L	micro-beam length,
u, w, φ	axial displacement, transverse displacement, rotation of mid-plane,
κ_s	shear correction factor,
l	length scale parameter,
E, ν	Young's modulus, Poisson's ratio,
A, B, D, F	material-dependent coefficients,
h	micro-beam thickness,
b	micro-beam width,
N_x	axial force,
Q_x	shear force,
M_x	bending moment,

ρ	density,
δ	Dirac delta distribution,
ξ	source point,
ψ_i	shape functions,
V	volume fraction,
λ	power-law index,
q	distributed load intensity,
H	unit step function.

1. Introduction

MANY PROBLEMS IN ENGINEERING SCIENCE ARE FORMULATED in terms of partial differential equations. Usually, analytical solutions do not exist or are more difficult to be derived due to the nature of the problem, domain of problem analysis, or boundary conditions. Thus, numerical methods are to be used to obtain approximate solutions of the governing differential equations. The boundary-element method is one of the numerical techniques, which employs fundamental solutions of certain partial differential equations as weight functions in weighted-residual statements. The nature of the fundamental solutions used in a boundary element formulation determines the main characteristics of the solution procedures. In the domain-boundary element method (D-BEM), fundamental solutions are independent of time and called static fundamental solutions. Utilization of static fundamental solutions results in a system of integral equations, which consists of domain integrals involving applied loads, time derivatives of unknown functions, and material couplings. There are certain advantages associated with the use of D-BEM in elastodynamic computations. Static fundamental solutions adopted in D-BEM are much simpler compared to time-dependent fundamental solutions employed in various boundary element techniques and D-BEM has better stability characteristics [1]. As a result, the high computational cost associated with time-domain BEM techniques can be reduced through the use of D-BEM. The CPU time in D-BEM is shown to be much less than that required in conventional techniques such as the finite difference method [2].

D-BEM has been used previously to solve a number of problems. CARRER *et al.* [1] employed the method to investigate the dynamic behavior of Timoshenko beams under various loadings. The study was further extended for dynamic analysis of functionally graded Timoshenko beams by ESHRAGHI and DAG [2] and laminated fiber-reinforced Timoshenko beams by AHMED *et al.* [3]. CARRER *et al.* [4, 5] used D-BEM to examine the 2D scalar wave propagation. The method was also applied for elastodynamic analysis of plates. Axisymmetric forced vibrations of functionally graded annular and circular plates were studied by ESHRAGHI and DAG [6]. PROVIDAKIS [7] presented a D-BEM approach for transient dynamic analysis of thick plates on a Winkler-type foundation.

HATZIGEORGIU and BESKOS [8], and PROVIDAKIS and BESKOS [9] proposed D-BEM based solutions for dynamic elastoplasticity of three dimensional structures and thin flexural plates, respectively. SOARES Jr. *et al.* [10] performed non-linear dynamic analysis by coupling D-BEM with the time-domain BEM. They used an iterative coupling scheme and the domain was divided into two sub-domains. The non-linear part of the problem was modelled by D-BEM. PETRES *et al.* [11] put forward a D-BEM based solution for heat diffusion, including heat generation and internal dissipation, in homogeneous and isotropic media. OYARZUN *et al.* [12] explicitly calculated Green's functions and incorporated them in the time marching scheme of D-BEM to develop a solution procedure with improved accuracy and stability.

Different formulations of the boundary element method are also proposed to carry out the dynamic analysis of structures. One such technique is the dual reciprocity boundary element method (DR-BEM), which employs static fundamental solutions in the analysis. KONTONI [13] presented a DR-BEM based procedure for dynamic analysis of elastoplastic problems. KÖGL and GAUL [14] examined three dimensional problems of transient piezoelectricity by the DR-BEM. The technique is adopted by CHIEN *et al.* [15] for the solution of two-dimensional elastodynamic problems. The implementation of the method for dynamic fracture mechanics is illustrated by ALBUQUERQUE *et al.* [16] and LU and WU [17]. USECHE and ALBUQUERQUE [18, 19] demonstrated applications of DR-BEM in dynamic structural mechanics. DR-BEM allows conversion of the domain integrals resulting from the use of the static fundamental solution to boundary integrals [14–16]. The method is deemed to be computationally efficient because of the use of the static fundamental solution and boundary-only discretization.

Another approach to carry out elastodynamic analysis in BEM is based on the derivation of fundamental solutions in the Laplace transform domain. WEN *et al.* [20] applied such a technique to study dynamic plate bending problems. WEN and ALIABADI [21] detailed the application of the boundary element frequency domain formulation for dynamic analysis of Mindlin plates. A similar approach is outlined by WEN and ALIABADI [22] to analyse a shear deformable plate resting on an elastic foundation. Three dimensional Laplace domain piezoelectric fundamental solutions are used by IGUMNOV *et al.* [23] to examine dynamic bending of a circular piezoelectric plate. Other applications of the boundary element method in dynamic analysis involve torsional vibrations [24, 25], half-space loaded by a moving time-dependent force [26], structural and acoustic response of composite plates [27], and two-dimensional elastodynamics [28, 29].

In both the domain-boundary element method and the dual reciprocity boundary element method, static fundamental solutions are used to develop the formulation. This approach leads to domain integrals in both procedures. These

integrals are converted to boundary integrals in DR-BEM, whereas in D-BEM they are treated by employing cells and domain discretization. The Laplace transform domain based formulation is also a boundary-only formulation, and makes use of fundamental solutions in the Laplace domain.

The objective of the present study is to develop a D-BEM based technique for forced vibration analysis of functionally graded micro-beams. The formulation is derived utilizing the modified couple stress theory. Functionally graded materials (FGMs) are advanced composites, that possess smooth spatial variations in the volume fractions of the constituent materials. The characteristic feature of FGMs is the inhomogeneity at both micro- and macro-scales. The inhomogeneity and continuous spatial variations of the physical properties need to be accounted for in theoretical and computational studies so as to produce realistic results regarding behavior of the graded structures.

There are a number of production technologies such as magnetron sputtering [30], plasma-enhanced chemical vapor deposition [31], and modified soft lithography [32] that make the use of functionally graded components in micro-electro-mechanical-systems (MEMSs) feasible. The analysis of such structures requires the use of higher order continuum theories that include the size effects. One of the most commonly used higher order continuum theory in the analysis of micro-structures is the modified couple stress theory [33]. A single length scale parameter is needed in this theory to describe a material response at the micro-scale. The modified couple stress theory based previous works on micro-beams include both homogeneous and functionally graded structures. MA *et al.* [34] developed a size-dependent Timoshenko beam model for homogeneous beams employing the modified couple stress theory. Functionally graded Timoshenko micro-beams were examined by ASGHARI *et al.* [35, 36]. Static bending and free vibration analysis of functionally graded micro-beams were carried out by ŞİMŞEK *et al.* [37] and ŞİMŞEK and REDDY [38], respectively. Effects of variable length-scale parameter on static bending and free vibrations of functionally graded beams were investigated by AGHAZADEH *et al.* [39]. BABAEI *et al.* [40] analyzed free vibrations of functionally graded micro-beams in thermal environments considering temperature dependent material properties.

There are various articles on forced vibrations of micro-beams. GHAYESH *et al.* [41] and VATANKHAH *et al.* [42] examined forced vibrations of micro-beams using strain gradient theory. Forced vibrations of bi-directional functionally graded beams carrying a moving mass was considered by RAJASEKARAN and BAKHSI KHANIKI [43] using the modified couple stress theory. Geometrically nonlinear forced vibrations of functionally graded micro-beams on a nonlinear elastic foundation was studied by DAS [44]. Nonlinear dynamics of functionally graded micro-beams was examined by SHENG and WANG [45] employing the von Kármán nonlinear theory and considering the material damping.

In the present study, governing partial differential equations for functionally graded micro-beams are derived by applying Hamilton's principle. The static fundamental solution for each of the governing PDE's is obtained by considering the corresponding reduced form. Fundamental solutions are then utilized as weight functions in the weighted residual statements. These statements are converted to a system of integral equations through integration by parts and algebraic manipulations. A system of time-dependent ordinary differential equations is then obtained via domain discretization and shape-function approximation. The Houbolt method [46, 47] is used in the numerical solution of the ordinary differential equations. The proposed methodology is applicable for homogeneous and functionally graded micro-beams with any kind of material variation profile. Furthermore, the method can be applied to ordinary Timoshenko beams by setting the length-scale parameter as zero. Developed procedures are verified by comparisons to solutions available in the literature. Parametric analyses are carried out for functionally graded micro-beams under time-dependent excitations such as step, harmonic, and impulsive loads. Presented computational results illustrate the effects of the inhomogeneity index and the length-scale parameter on a forced vibration response of functionally graded micro-beams.

2. Equations of motion and boundary conditions

Figure 1 shows the geometry of a functionally graded Timoshenko micro-beam under general time-dependent loading $q(x, t)$. Length, height, and width of the beam are respectively denoted by L , h , and b . All material properties of the beam are assumed to be continuous functions of the thickness coordinate z . As also shown in Fig. 1, transverse shear strain γ_{xz} is presumed constant across the thickness in the Timoshenko beam theory, and the displacement field is expressed as follows:

$$(2.1) \quad u_x(x, z, t) = u(x, t) - z\varphi(x, t),$$

$$(2.2) \quad u_y(x, z, t) = 0,$$

$$(2.3) \quad u_z(x, z, t) = w(x, t),$$

where u_x , u_y and u_z are scalar displacement components; u and w are mid-plane displacements; φ is mid-plane rotation, and t is time. Applying the small-strain theory, non-zero strains can be found as:

$$(2.4) \quad \varepsilon_{xx}(x, z, t) = \frac{\partial u(x, t)}{\partial x} - z \frac{\partial \varphi(x, t)}{\partial x},$$

$$(2.5) \quad \varepsilon_{xz}(x, z, t) = \frac{1}{2} \left[\frac{\partial w(x, t)}{\partial x} - \varphi(x, t) \right].$$

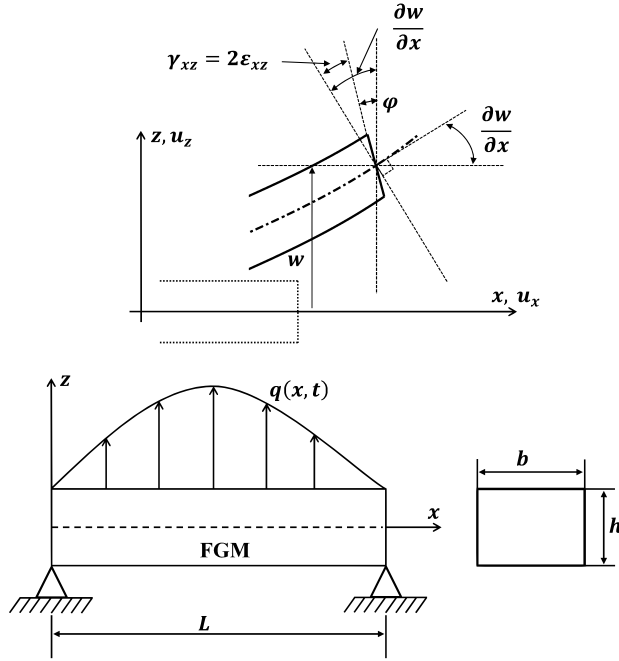


FIG. 1. Functionally graded Timoshenko micro-beam and deformed shape.

Generalized Hooke’s law results in the following expressions for non-zero stresses:

$$(2.6) \quad \sigma_{xx}(x, z, t) = [2\mu(z) + \lambda(z)]\epsilon_{xx}(x, z, t),$$

$$(2.7) \quad \sigma_{yy}(x, z, t) = \sigma_{zz}(x, z, t) = \lambda(z)\epsilon_{xx}(x, z, t),$$

$$(2.8) \quad \sigma_{xz}(x, z, t) = 2\kappa_s\mu(z)\epsilon_{xz}(x, z, t),$$

where $\mu(z)$ and $\lambda(z)$ are Lamé’s parameters, which are functions of the z -coordinate. κ_s is the shear correction factor specified as $5/6$ for a rectangular cross-section.

In modified couple stress theory, non-zero component of symmetric curvature tensor and the corresponding non-zero component of the deviatoric part of the couple stress tensor are respectively given by:

$$(2.9) \quad \chi_{xy}(x, z, t) = -\frac{1}{4} \left[\frac{\partial^2 w(x, t)}{\partial x^2} + \frac{\partial \varphi(x, t)}{\partial x} \right],$$

$$(2.10) \quad m_{xy}(x, z, t) = 2\mu(z)l^2(z)\chi_{xy}(x, z, t),$$

where $l(z)$ is the length scale parameter, which is a function of the thickness coordinate z . Following the procedure described in [39], i.e. applying Hamilton’s

principle in conjunction with Eqs. (2.1)–(2.10) and using integration by parts, governing partial differential equations for elastodynamics of the FGM Timoshenko micro-beam are derived as follows:

$$(2.11) \quad A_{11}u_{,xx} - B_{11}\varphi_{,xx} = I_1\ddot{u} - I_2\ddot{\varphi},$$

$$(2.12) \quad -\frac{A_{552}}{4}(w_{,xxxx} + \varphi_{,xxx}) + \kappa_s F_{55}(w_{,xx} - \varphi_{,x}) + q = I_1\ddot{w},$$

$$(2.13) \quad D_{11}\varphi_{,xx} + \frac{A_{552}}{4}(w_{,xxx} + \varphi_{,xx}) + \kappa_s F_{55}(w_{,x} - \varphi) - B_{11}u_{,xx} = I_3\ddot{\varphi} - I_2\ddot{u},$$

where a dot over a variable indicates differentiation with respect to time. The coefficients of the equations depend on through-the-thickness integrals of material properties and are given by:

$$(2.14) \quad \{A_{11}, B_{11}, D_{11}\} = \int_{-h/2}^{h/2} \frac{E(z)[1 - \nu(z)]}{[1 + \nu(z)][1 - 2\nu(z)]} \{1, z, z^2\} b dz,$$

$$(2.15) \quad F_{55} = \int_{-h/2}^{h/2} \frac{E(z)}{2[1 + \nu(z)]} b dz,$$

$$(2.16) \quad A_{552} = \int_{-h/2}^{h/2} \frac{l^2(z)E(z)}{2[1 + \nu(z)]} b dz,$$

$$(2.17) \quad \{I_1, I_2, I_3\} = \int_{-h/2}^{h/2} \rho(z) \{1, z, z^2\} b dz.$$

The functions $E(z)$, $\nu(z)$, and $\rho(z)$ in the integrands, respectively stand for modulus of elasticity, Poisson’s ratio, and density.

Related essential boundary conditions at ends of the beam are:

$$(2.18) \quad u(x, t) = \bar{u}(x, t),$$

$$(2.19) \quad w(x, t) = \bar{w}(x, t),$$

$$(2.20) \quad w_{,x}(x, t) = \bar{w}_{,x}(x, t),$$

$$(2.21) \quad \varphi(x, t) = \bar{\varphi}(x, t),$$

and natural boundary conditions are given as:

$$(2.22) \quad N_x = -A_{11}u_{,x} + B_{11}\varphi_{,x} = \bar{N}_x,$$

$$(2.23) \quad Q_x = \frac{A_{552}}{4}(w_{,xxx} + \varphi_{,xx}) - \kappa_s F_{55}(w_{,x} - \varphi) = \bar{Q}_x,$$

$$(2.24) \quad R_x = -\frac{A_{552}}{4}(w_{,xx} + \varphi_{,x}) = \bar{R}_x,$$

$$(2.25) \quad M_x = -\frac{A_{552}}{4}(w_{,xx} + \varphi_{,x}) - D_{11}\varphi_{,x} + B_{11}u_{,x} = \bar{M}_x,$$

where a bar over a variable indicates a prescribed value.

3. Domain-boundary element method

In order to convert the governing partial differential equations into integral forms, static fundamental solutions are required to be used in weighted-residual expressions. These solutions can be obtained by considering the following reduced forms of the original partial differential equations [1]:

$$(3.1) \quad A_{11}u_{,xx}^*(x, \xi) = \delta(x - \xi),$$

$$(3.2) \quad -\frac{A_{552}}{4}\left(w_{,xxxx}^* - \frac{\kappa_s F_{55}}{A_{552}/4}w_{,xx}^*\right) = \delta(x - \xi),$$

$$(3.3) \quad \left(D_{11} + \frac{A_{552}}{4}\right)\left[\varphi_{,xx}^*(x, \xi) - \frac{\kappa_s F_{55}}{D_{11} + A_{552}/4}\varphi^*(x, \xi)\right] = \delta(x - \xi),$$

where $\delta(x - \xi)$ is the Dirac delta distribution; and $u^*(x, \xi)$, $w^*(x, \xi)$, and $\varphi^*(x, \xi)$ are static fundamental solutions. Solving these equations, fundamental solutions are derived as follows:

$$(3.4) \quad u^*(x, \xi) = \frac{1}{A_{11}} \frac{|x - \xi|}{2},$$

$$(3.5) \quad w^*(x, \xi) = \frac{1}{\Lambda_w A_{552}/4} \left\{ \frac{|x - \xi|}{2} - \frac{\sinh[\sqrt{\Lambda_w}|x - \xi|]}{2\sqrt{\Lambda_w}} \right\},$$

$$(3.6) \quad \varphi^*(x, \xi) = \frac{1}{D_{11} + A_{552}/4} \frac{\sinh[\sqrt{\Lambda_\varphi}|x - \xi|]}{2\sqrt{\Lambda_\varphi}}.$$

In these equations, $\Lambda_w = 4\kappa_s F_{55}/A_{552}$ and $\Lambda_\varphi = \kappa_s F_{55}(D_{11} + A_{552}/4)$. Note that in the derivation of the above fundamental solutions, we have used the following identities:

$$(3.7) \quad \frac{d}{dx}|x - \xi| = \text{sgn}(x - \xi) = \begin{cases} -1 & \text{if } x < \xi, \\ 1 & \text{if } x > \xi, \end{cases}$$

$$(3.8) \quad \text{sgn}(x - \xi) = 2H(x - \xi) - 1,$$

$$(3.9) \quad \frac{d}{dx}H(x - \xi) = \delta(x - \xi),$$

where sgn is the sign function and $H(x - \xi)$ is the Heaviside step function.

Using the static fundamental solutions as weight functions, weighted residual statements, i.e., weak forms of the governing partial differential equations are written as follows:

$$(3.10) \quad \int_0^L [A_{11}u_{,xx} - B_{11}\varphi_{,xx} - I_1\ddot{u} + I_2\ddot{\varphi}]u^*(x, \xi) dx = 0,$$

$$(3.11) \quad \int_0^L \left[-\frac{A_{552}}{4}(w_{,xxxx} + \varphi_{,xxx}) + \kappa_s F_{55}(w_{,xx} - \varphi_{,x}) + q - I_1\ddot{w} \right] \times w^*(x, \xi) dx = 0,$$

$$(3.12) \quad \int_0^L \left[D_{11}\varphi_{,xx} + \frac{A_{552}}{4}(w_{,xxx} + \varphi_{,xx}) + \kappa_s F_{55}(w_{,x} - \varphi) - B_{11}u_{,xx} - I_3\ddot{\varphi} + I_2\ddot{u} \right] \varphi^*(x, \xi) dx = 0.$$

Equations (3.10)–(3.12) can be expressed in terms of boundary conditions and domain integrals. To illustrate this, we consider Eq. (3.10). Performing integration by parts, the first two terms are written as:

$$(3.13) \quad \int_0^L [A_{11}u_{,xx} - B_{11}\varphi_{,xx}]u^*(x, \xi) dx = \{[A_{11}u_{,x} - B_{11}\varphi_{,x}]u^*(x, \xi)\}_0^L - \int_0^L [A_{11}u_{,x} - B_{11}\varphi_{,x}]u^*_{,x}(x, \xi) dx.$$

We perform another integration by parts for the integral on the right side, which is expressed as:

$$(3.14) \quad \int_0^L [A_{11}u_{,x} - B_{11}\varphi_{,x}]u^*_{,x}(x, \xi) dx = \{[A_{11}u - B_{11}\varphi]u^*_{,x}(x, \xi)\}_0^L - \int_0^L [A_{11}u - B_{11}\varphi]u^*_{,xx}(x, \xi) dx.$$

Note that from Eq. (3.1) it follows that $u^*_{,xx}(x, \xi) = \delta(x - \xi)/A_{11}$. Using the properties of the $\delta(x - \xi)$ one can then write:

$$(3.15) \quad \int_0^L [A_{11}u - B_{11}\varphi]u^*_{,xx}(x, \xi) dx = \int_0^L [A_{11}u - B_{11}\varphi] \frac{\delta(x - \xi)}{A_{11}} dx = u(\xi, t) - \frac{B_{11}}{A_{11}}\varphi(\xi, t).$$

Thus,

$$\begin{aligned}
 (3.16) \quad & \int_0^L [A_{11}u_{,xx} - B_{11}\varphi_{,xx}]u^*(x, \xi) dx \\
 & = u(\xi, t) - \frac{B_{11}}{A_{11}}\varphi(\xi, t) + \{[A_{11}u_{,x} - B_{11}\varphi_{,x}]u^*(x, \xi)\}_0^L \\
 & \quad - \{[A_{11}u - B_{11}\varphi]u^*_{,x}(x, \xi)\}_0^L.
 \end{aligned}$$

Pursuing a procedure similar to that explained for Eq. (3.10) and elaborated in [2] for Eqs. (3.11) and (3.12), i.e. applying integration by parts twice to Eqs. (3.11) and (3.12), utilizing the properties of the Dirac delta distribution, and employing Eqs. (2.22)–(2.25), Eqs. (3.10)–(3.12) are recast into the following forms:

$$\begin{aligned}
 (3.17) \quad & u(\xi, t) - \frac{B_{11}}{A_{11}}\varphi(\xi, t) \\
 & = [u^*(x, \xi)N_x(x, t)]_{x=0}^{x=L} + \{u^*_{,x}(x, \xi)[A_{11}u(x, t) - B_{11}\varphi(x, t)]\}_{x=0}^{x=L} \\
 & \quad + \int_0^L u^*(x, \xi)[I_1\ddot{u}(x, t) - I_2\ddot{\varphi}(x, t)] dx,
 \end{aligned}$$

$$\begin{aligned}
 (3.18) \quad & w(\xi, t) = [w^*(x, \xi)Q_x(x, t)]_{x=0}^{x=L} + [w^*_{,x}(x, \xi)R_x(x, t)]_{x=0}^{x=L} \\
 & \quad + \left\{ \left[\kappa_s F_{55} w^*_{,x}(x, \xi) - \frac{A_{552}}{4} w^*_{,xxx}(x, \xi) \right] w(x, t) \right\}_{x=0}^{x=L} \\
 & \quad - \int_0^L \left[\kappa_s F_{55} w^*(x, \xi) + \frac{A_{552}}{4} w^*_{,xxx}(x, \xi) \right] \varphi(x, t) dx \\
 & \quad + \left\{ \frac{A_{552}}{4} w^*_{,xx}(x, \xi) [w_{,x}(x, t) + \varphi(x, t)] \right\}_{x=0}^{x=L} \\
 & \quad - \int_0^L w^*(x, \xi) q(x, t) dx + \int_0^L I_1 w^*(x, \xi) \ddot{w}(x, t) dx,
 \end{aligned}$$

$$\begin{aligned}
 (3.19) \quad & \varphi(\xi, t) - \frac{B_{11}}{D_{11} + A_{552}/4} u(\xi, t) + \frac{A_{552}/4}{D_{11} + A_{552}/4} w_{,x}(\xi, t) \\
 & = [\varphi^*(x, \xi)M_x(x, t)]_{x=0}^{x=L} \\
 & \quad - \left\{ \varphi^*_{,x}(x, \xi) \left[B_{11}u(x, t) - \frac{A_{552}}{4} w_{,x}(x, t) - \left(D_{11} + \frac{A_{552}}{4} \right) \varphi(x, t) \right] \right\}_{x=0}^{x=L} \\
 & \quad - \left[\left(\frac{A_{552}}{4} \Lambda_\varphi + \kappa_s F_{55} \right) \varphi^*(x, \xi) w(x, t) \right]_{x=0}^{x=L}
 \end{aligned}$$

$$\begin{aligned}
 &+ \int_0^L \left(\frac{A_{552}}{4} \Lambda_\varphi + \kappa_s F_{55} \right) \varphi_{,x}^*(x, \xi) w(x, t) dx \\
 &+ \int_0^L B_{11} \Lambda_\varphi \varphi^*(x, \xi) u(x, t) dx - \int_0^L \varphi^*(x, \xi) [I_2 \ddot{u}(x, t) - I_3 \ddot{\varphi}(x, t)] dx.
 \end{aligned}$$

Note that the problem involves eight boundary unknowns and solution requires four distinct integral equations. The additional equation can be obtained by taking the derivative of Eq. (3.18) with respect to the source point ξ . This leads to an integral equation for $w_{,x}$. Performing this operation and substituting the fundamental solution expressions from Eqs. (3.4)–(3.6) into Eqs. (3.17)–(3.19), final forms of the integral equations are found as given below:

$$\begin{aligned}
 (3.20) \quad &u(\xi, t) - \frac{1}{2} [u(0, t) + u(L, t)] - \frac{B_{11}}{A_{11}} \varphi(\xi, t) + \frac{B_{11}}{2A_{11}} [\varphi(0, t) + \varphi(L, t)] \\
 &= \frac{1}{2A_{11}} [N_x(L, t)(L - \xi) - N_x(0, t)\xi] + \frac{1}{2A_{11}} \int_0^L |x - \xi| [I_1 \ddot{u}(x, t) - I_2 \ddot{\varphi}(x, t)] dx,
 \end{aligned}$$

$$\begin{aligned}
 (3.21) \quad &w(\xi, t) - \frac{1}{2} [w(0, t) + w(L, t)] + \frac{\sinh[\sqrt{\Lambda_w}(L - \xi)]}{2\sqrt{\Lambda_w}} [w_{,x}(L, t) + \varphi(L, t)] \\
 &- \frac{\sinh[\sqrt{\Lambda_w}\xi]}{2\sqrt{\Lambda_w}} [w_{,x}(0, t) + \varphi(0, t)] \\
 &+ \int_0^L \operatorname{sgn}(x - \xi) \left[\frac{1}{2} - \cosh(\sqrt{\Lambda_w}|x - \xi|) \right] \varphi(x, t) dx \\
 &= \frac{1}{\kappa_s F_{55}} \left\{ Q_x(L, t) \left(\frac{L - \xi}{2} - \frac{\sinh[\sqrt{\Lambda_w}(L - \xi)]}{2\sqrt{\Lambda_w}} \right) - Q_x(0, t) \left(\frac{\xi}{2} - \frac{\sinh[\sqrt{\Lambda_w}\xi]}{2\sqrt{\Lambda_w}} \right) \right\} \\
 &+ \frac{1}{\kappa_s F_{55}} \left\{ R_x(L, t) \left(\frac{1 - \cosh[\sqrt{\Lambda_w}(L - \xi)]}{2} \right) + R_x(0, t) \left(\frac{1 - \cosh[\sqrt{\Lambda_w}\xi]}{2} \right) \right\} \\
 &- \frac{1}{\kappa_s F_{55}} \int_0^L \left\{ \frac{|x - \xi|}{2} - \frac{\sinh[\sqrt{\Lambda_w}|x - \xi|]}{2\sqrt{\Lambda_w}} \right\} [q(x, t) - I_1 \ddot{w}(x, t)] dx,
 \end{aligned}$$

$$\begin{aligned}
 (3.22) \quad &w_{,x}(\xi, t) + \varphi(\xi, t) - \frac{\cosh[\sqrt{\Lambda_w}(L - \xi)]}{2} [w_{,x}(L, t) + \varphi(L, t)] \\
 &- \frac{\cosh[\sqrt{\Lambda_w}\xi]}{2} [w_{,x}(0, t) + \varphi(0, t)] + \int_0^L \sqrt{\Lambda_w} \sinh(\sqrt{\Lambda_w}|x - \xi|) \varphi(x, t) dx
 \end{aligned}$$

$$\begin{aligned}
&= \frac{1}{\kappa_s F_{55}} \left\{ Q_x(L, t) \left(-\frac{1}{2} + \frac{\cosh[\sqrt{\Lambda_w}(L-\xi)]}{2} \right) - Q_x(0, t) \left(\frac{1}{2} - \frac{\cosh[\sqrt{\Lambda_w}\xi]}{2} \right) \right\} \\
&+ \frac{1}{\kappa_s F_{55}} \left\{ R_x(L, t) \left(\frac{\sqrt{\Lambda_w} \sinh[\sqrt{\Lambda_w}(L-\xi)]}{2} \right) + R_x(0, t) \left(\frac{-\sqrt{\Lambda_w} \sinh[\sqrt{\Lambda_w}\xi]}{2} \right) \right\} \\
&- \frac{1}{\kappa_s F_{55}} \int_0^L \operatorname{sgn}(x-\xi) \left\{ -\frac{1}{2} + \frac{\cosh[\sqrt{\Lambda_w}|x-\xi|]}{2} \right\} [q(x, t) - I_1 \ddot{w}(x, t)] dx,
\end{aligned}$$

$$\begin{aligned}
(3.23) \quad &\varphi(\xi, t) - \frac{B_{11}}{D_{11} + A_{552}/4} u(\xi, t) + \frac{A_{552}/4}{D_{11} + A_{552}/4} w_{,x}(\xi, t) \\
&+ \frac{\cosh[\sqrt{\Lambda_\varphi}(L-\xi)]}{2(D_{11} + A_{552}/4)} \left[B_{11} u(L, t) - \frac{A_{552}}{4} w_{,x}(L, t) - \left(D_{11} + \frac{A_{552}}{4} \right) \varphi(L, t) \right] \\
&+ \frac{\cosh[\sqrt{\Lambda_\varphi}\xi]}{2(D_{11} + A_{552}/4)} \left[B_{11} u(0, t) - \frac{A_{552}}{4} w_{,x}(0, t) - \left(D_{11} + \frac{A_{552}}{4} \right) \varphi(0, t) \right] \\
&+ \sqrt{\Lambda_\varphi} \left(1 + \frac{A_{552}/4}{D_{11} + A_{552}/4} \right) \left\{ \frac{\sinh[\sqrt{\Lambda_\varphi}(L-\xi)]}{2} w(L, t) - \frac{\sinh[\sqrt{\Lambda_\varphi}\xi]}{2} w(0, t) \right\} \\
&- \Lambda_\varphi \left(1 + \frac{A_{552}/4}{D_{11} + A_{552}/4} \right) \int_0^L \operatorname{sgn}(x-\xi) \frac{\cosh(\sqrt{\Lambda_\varphi}|x-\xi|)}{2} w(x, t) dx \\
&- \frac{B_{11} \sqrt{\Lambda_\varphi}}{D_{11} + A_{552}/4} \int_0^L \frac{\sinh(\sqrt{\Lambda_\varphi}|x-\xi|)}{2} u(x, t) dx \\
&= \frac{1}{D_{11} + A_{552}/4} \left\{ M_x(L, t) \frac{\sinh[\sqrt{\Lambda_\varphi}(L-\xi)]}{2\sqrt{\Lambda_\varphi}} - M_x(0, t) \frac{\sinh[\sqrt{\Lambda_\varphi}\xi]}{2\sqrt{\Lambda_\varphi}} \right\} \\
&- \frac{1}{D_{11} + A_{552}/4} \int_0^L \frac{\sinh[\sqrt{\Lambda_\varphi}|x-\xi|]}{2\sqrt{\Lambda_\varphi}} [I_2 \ddot{u}(x, t) - I_3 \ddot{\varphi}(x, t)] dx.
\end{aligned}$$

In order to be able to calculate domain integrals appearing in Eqs. (3.20)–(3.23), the beam is discretized into a finite number of quadratic cells, each of which has three nodes as shown in Fig. 2. A total of N equally spaced nodes are employed. The domain enclosed by three consecutive nodes is a cell, thus there are a total of $M = (N - 1)/2$ cells. The j^{th} cell covers the interval $\Omega_j = [x_1^j, x_3^j]$, $1 \leq j \leq M$; x_1^j and x_3^j being the x coordinate of the first and last node of the j^{th} cell, respectively. The x -coordinate of the middle node of the j^{th} cell is denoted by x_2^j .

Second-order polynomial shape functions are used to approximate the variation of a quantity over a cell. The shape functions are given by:

$$(3.24) \quad \psi_1^j(x) = \frac{(x - x_2^j)(x - x_3^j)}{2h_c^2},$$

$$(3.25) \quad \psi_2^j(x) = -\frac{(x - x_1^j)(x - x_3^j)}{h_c^2},$$

$$(3.26) \quad \psi_3^j(x) = \frac{(x - x_1^j)(x - x_2^j)}{2h_c^2},$$

where h_c is the half-length of each cell.

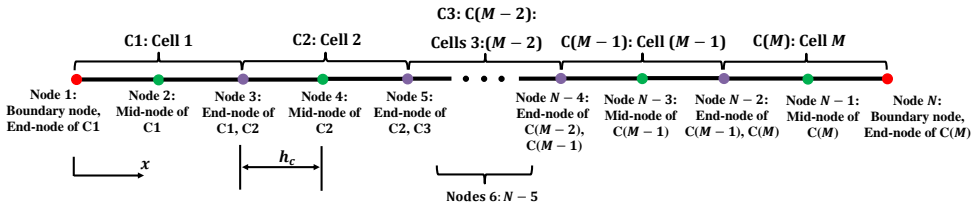


FIG. 2. Domain discretization.

Variation of a generic variable ζ across the cell is approximated as follows:

$$(3.27) \quad \zeta = \sum_{i=1}^3 \psi_i^j(x) \zeta(x_i^j, t).$$

The function value $\zeta(x_i^j, t)$ is calculated at the i^{th} node of the j^{th} cell at time t . Using the approximation introduced by (3.27), the domain integrals in Eqs. (3.20)–(3.23) are computed over each cell and the results are added up to estimate the total value. Applying this discretization, a generic domain integral can be expressed as follows:

$$(3.28) \quad \int_0^L \eta^*(x, \xi) \zeta(x, t) dx = \sum_{j=1}^M \int_{x_1^j}^{x_3^j} \eta^*(x, \xi) \left[\sum_{i=1}^3 \psi_i^j(x) \zeta(x_i^j, t) \right] dx,$$

where $\eta^*(x, \xi)$ is any of the fundamental solutions in Eqs. (3.4)–(3.6) or its derivative with respect to x ; and $\zeta(x, t)$ stands for either an unknown displacement function or its second time derivative.

A set of ordinary differential equations in time is obtained by writing each of Eqs. (3.20)–(3.23) for every boundary node $\xi_k = (0, L)$, ($k = 1, N$); and for every internal node $\xi_k = (h_c, 2h_c, \dots, L - h_c)$ ($k = 2, 3, \dots, N - 1$). Then, the equations are consolidated into the following matrix form:

$$(3.29) \quad [\mathbf{A}]\{u\} = [\mathbf{S}]\{\ddot{u}\} + [\mathbf{G}]\{N\} + \{f\}.$$

All vectors and matrices in Eq. (3.29) are given in Appendices A–C. The time-dependent system of ordinary differential equations given by Eq. (3.29) is solved by means of the Houbolt method.

In the Houbolt method, variation of a parameter from $t = t_{n-2}$ to $t = t_{n+1}$ is approximated by cubic Lagrange interpolation. The following representation is applied to calculate the second time derivative of a generic variable χ :

$$(3.30) \quad \ddot{\chi}_{n+1} = \frac{1}{\Delta t^2} [2\chi_{n+1} - 5\chi_n + 4\chi_{n-1} - \chi_{n-2}].$$

There are various time integration schemes such as the Newmark method, the Wilson ϑ -method, and the Houbolt method, that yield accurate results for linear structural dynamics problems [48]. The Newmark method is a universal and reliable method that makes use of displacement, velocity, and acceleration at the previous time step. However, it may require longer calculation time compared to the Houbolt method, which is an algorithm that involves a starting procedure. The system does not decouple when the Houbolt method is applied. The Houbolt method is an implicit method, whereas the Newmark method can be implicit or explicit depending on the choice of the parameters. Furthermore, the Houbolt method is a three-step method, and it is shown to be unconditionally stable [49].

Equation (3.29) can be used to solve static bending, and free and forced vibrations problems of functionally graded micro-beams. For the static problem $\{\ddot{u}\} = 0$ and we have:

$$(3.31) \quad [\mathbf{A}]\{u\} = [\mathbf{G}]\{N\} + \{f\}.$$

The solution of Eq. (3.31) yields static nodal displacements and unknown natural boundary values. For the free vibration problem we take $\{f\} = 0$, and assume that $\{u(x, t)\} = \{U(x)\} \exp(i\Omega t)$. From Eqs. (2.22)–(2.25), we conclude that $\{N\} = \{N^*\} \exp(i\Omega t)$. Substitution of these expressions back into Eq. (3.29) yields:

$$(3.32) \quad ([\mathbf{A}]\{U\} - [\mathbf{G}]\{N^*\})e^{i\Omega t} + \Omega^2[\mathbf{S}]\{\ddot{U}\}e^{i\Omega t} = 0.$$

This is an eigenvalue problem whose solution yields natural frequencies and corresponding mode-shapes for free vibrations of functionally graded micro-beams.

4. Numerical results

The geometry of the functionally graded beam considered in parametric analyses is shown in Fig. 1. The micro-beam is assumed to be a mixture of ceramic and metal. One of the approximate ways of calculating elastic properties of functionally graded materials is the use of a micromechanics approach such as

the Mori–Tanaka model [50], which gives the bulk modulus of a two-phase composite consisting of spherical inclusions in a matrix material. The approximation stems from the fact that the concept of a representative volume element (RVE) cannot be unique for functionally graded materials [51]. This is a consequence of spatial variations in all material properties. However, as illustrated in previous studies, the Mori–Tanaka method can be used to evaluate the elastic properties with reasonable accuracy. For example, the article by SHEN and WANG [52] indicates that the difference between free vibration analysis results generated by Voigt and Mori–Tanaka micromechanics models is either very small or negligible. For this reason, the Mori–Tanaka micromechanics model is commonly used in vibration analyses of FGMs [53–55]. The length scale parameter in small-scale analyses is primarily defined as a representative size of small-scale effect near an interface, a surface, or a singular point such as a crack [56]. The RVE size of any micromechanics model is expected to be smaller than the length scale parameter. Since the Mori–Tanaka approach is not extended for small-scale effects, a rule of mixtures type representation is adopted to describe the variation in the length scale parameter.

Thus, modulus of elasticity and Poisson’s ratio of the graded beam are computed in accordance with the Mori–Tanaka micromechanics model [50], and expressed as:

$$(4.1) \quad E(z) = \frac{9B_e(z)\mu_e(z)}{3B_e(z) + \mu_e(z)},$$

$$(4.2) \quad \nu(z) = \frac{3B_e(z) - 2\mu_e(z)}{6B_e(z) + 2\mu_e(z)},$$

where B_e and μ_e are respectively, effective bulk modulus and shear modulus; and written as follows:

$$(4.3) \quad B_e(z) = \frac{V_c(z)(B_c - B_m)}{1 + \frac{(B_c - B_m)V_m(z)}{(4\mu_m)/3 + B_m}} + B_m,$$

$$(4.4) \quad \mu_e(z) = \frac{V_c(z)(\mu_c - \mu_m)}{1 + \frac{(\mu_c - \mu_m)V_m(z)}{\{\mu_m + ((9B_m + 8\mu_m)\mu_m)/(6(B_m + 2\mu_m))\}}} + \mu_m.$$

Subscripts c and m in Eqs. (4.3) and (4.4) designate ceramic and metallic phases; and V stands for the volume fraction. Rule of mixtures is used to represent variations of mass density and length scale parameter in the following forms:

$$(4.5) \quad \rho(z) = \rho_m V_m(z) + \rho_c V_c(z),$$

$$(4.6) \quad l(z) = l_m V_m(z) + l_c V_c(z).$$

Spatial variation in the ceramic volume fraction is represented by a power function:

$$(4.7) \quad V_c(z) = \left(\frac{z}{h} + \frac{1}{2} \right)^\lambda.$$

The exponent λ is defined as power-law index. Sum of the volume fractions is equal to one, i.e.,

$$(4.8) \quad V_c(z) + V_m(z) = 1.$$

Thus, the beam is 100% metallic at $z = -h/2$, and 100% ceramic at $z = h/2$. Metallic and ceramic components of the FGM beam are assumed to be aluminum (Al) and silicon carbide (SiC), properties of which are given as:

$$(4.9) \quad E_m = 70 \text{ GPa}, \quad \nu_m = 0.3, \quad \rho_m = 2702 \text{ kg/m}^3, \quad l_m = 15 \text{ }\mu\text{m},$$

$$(4.10) \quad E_c = 427 \text{ GPa}, \quad \nu_c = 0.17, \quad \rho_c = 3100 \text{ kg/m}^3.$$

The length scale parameter ratio l_c/l_m is varied in parametric analyses to examine its effect on the dynamic response of the micro-beam. Geometric properties of the micro-beam are specified as:

$$(4.11) \quad h = 30 \text{ }\mu\text{m}, \quad b = 2h, \quad L = 10h, \quad \kappa_s = 5/6.$$

4.1. Verification

The accuracy of the static bending solution is verified by comparing our results regarding static deflection of a small-scale functionally graded beam pinned at both ends and subjected to uniformly distributed loading to those found through the differential quadrature method (DQM), and given by AGHAZADEH *et al.* [39]. Material properties of the beam are given by Eqs. (4.9) and (4.10). The results are provided in Fig. 3. There is excellent agreement between our results and those given by AGHAZADEH *et al.* [39].

A second set of comparisons is generated considering the results available in the literature for natural frequencies of functionally graded micro-beams. Table 1 shows the comparisons of dimensionless natural frequencies to those provided by ANSARI *et al.* [57] and AGHAZADEH *et al.* [39]. The dimensionless natural frequency is $\omega = \Omega L \sqrt{I_{10}/A_{110}}$ where Ω is the natural frequency of the beam and A_{110} and I_{10} are respectively reference values of A_{11} and I_1 evaluated by considering a fully metallic homogeneous beam. The frequencies presented correspond to the transverse deformation mode of the micro-beam. Results of first and fifth frequencies are compared with those reported in [39] and [57]. Results of second to fourth dimensionless natural frequencies are also reported in the table.

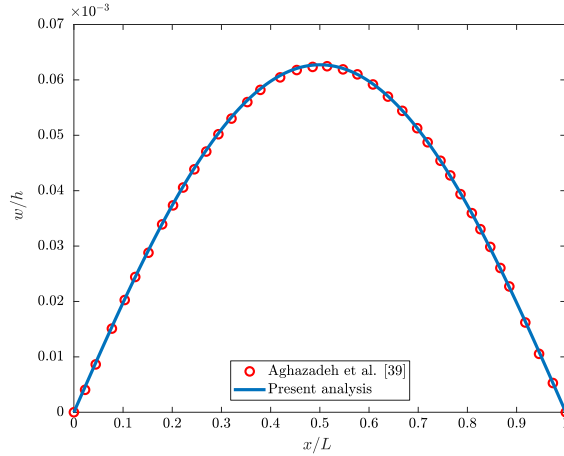


FIG. 3. Comparison of the static deflection curves for a functionally graded micro-beam with $L/h = 10$, $l_m = 15 \mu\text{m}$, $h/l_m = 2$, $b/h = 2$, $l_c/l_m = 3/2$, $\lambda = 2$.

The material length scale parameter is assumed to be constant and is taken as $l_c = l_m = 15 \mu\text{m}$. Again, almost an exact correspondence is observed between the results of present paper with those given in [39] and [57]. The maximum relative difference between the results of the current study and those reported in [57] is 1.7% for the first mode and 1.33% for the fifth mode. These differences are calculated for a pure metallic beam. For all other material distributions, the relative differences between our results and those given in [57] are less than 0.07%. However, the results of current study are in complete agreement with those reported in [39].

Table 1. Comparisons of the dimensionless natural frequency $\omega = \Omega L \sqrt{I_{10}/A_{110}}$ corresponding to the transverse deformation mode of FGM micro-beams with $l_c = l_m = 15 \mu\text{m}$, $h/l = 2$, $L/h = 10$.

Mode	Study	Material Type							Maximal relative difference (%)
		Pure ceramic	FGM ($\lambda = 0.1$)	FGM ($\lambda = 0.6$)	FGM ($\lambda = 1.2$)	FGM ($\lambda = 2$)	FGM ($\lambda = 10$)	Pure metal	
First	[57]	0.8538	0.7619	0.6084	0.5470	0.5100	0.4332	0.3863	1.7
	[39]	0.8538	–	0.6084	0.5469	0.5099	–	0.3797	0
	Present	0.8538	0.7624	0.6084	0.5469	0.5099	0.4330	0.3797	–
Second	Present	3.2551	2.9075	2.3167	2.0772	1.9306	1.6269	1.4323	–
Third	Present	6.8575	6.1276	4.8744	4.3570	4.0344	3.3684	2.9789	–
Fourth	Present	11.3360	10.1335	8.0502	7.1748	6.6200	5.4775	4.8636	–
Fifth	[57]	16.4672	14.7194	11.6879	10.3919	9.5590	7.8479	7.0831	1.33
	[39]	16.4671	–	11.6880	10.3916	9.5585	–	6.9886	0
	Present	16.4671	14.7264	11.6880	10.3916	9.5585	7.8452	6.9886	–

The dynamic beam response is examined for three different types of loading including distributed, concentrated, and impulsive loads. Forcing functions are expressed as follows:

$$(4.12) \quad q = q_0 H(t) \quad \text{for distributed step loading,}$$

$$(4.13) \quad q = P\delta(x - x_0) \sin(\omega_p t) \quad \text{for concentrated harmonic loading,}$$

$$(4.14) \quad q = P\delta(x - x_0)\delta(t) \quad \text{for concentrated impulsive loading,}$$

where $H(t)$ is the unit step function.

Calculation of the response for impulsive loading involves two steps. First the temporal derivative of $\{u\}$ at $t = 0$, i.e. $\{\dot{u}(x, 0)\}$, is obtained by time integration of Eq. (3.31) from $t = 0^-$ to $t = 0^+$:

$$(4.15) \quad \int_{0^-}^{0^+} ([\mathbf{A}]\{u\}) dt = \int_{0^-}^{0^+} ([\mathbf{S}]\{\ddot{u}\} + [\mathbf{G}]\{N\} + \{f\}) dt,$$

$\{u\}$ and $\{N\}$ are finite and their time integral in Eq. (4.15) is equal to zero. Since the loading is impulsive, $\{f\} = \{f^*\}\delta(t)$, and we may write:

$$(4.16) \quad [\mathbf{S}](\{\dot{u}\}_{0^+} - \{\dot{u}\}_{0^-}) = - \int_{0^-}^{0^+} \{f^*\}\delta(t) dt = -\{f^*\},$$

where $\{f^*\}$ is the spatially discretized form of the concentrated impulsive force, and is given in Appendix C. Also, note that $\{\dot{u}\}_{0^-} = \{0\}$. Solution of Eq. (4.16) yields $\{\dot{u}(x, 0)\}$. Designating $\{u(x, 0)\}$ and $\{\dot{u}(x, 0)\}$ by u_0 and \dot{u}_0 , respectively, and utilizing the backward central difference method, the following relations are derived to approximate u_{-1} and u_{-2} in the initialization of the Houbolt method:

$$(4.17) \quad u_{-1} = u_0 - \dot{u}_0 \Delta t,$$

$$(4.18) \quad u_{-2} = u_0 - 2\dot{u}_0 \Delta t.$$

Since analytical results regarding forced vibrations of micro-beams are not available in the literature, the verification study for forced vibrations is carried out by considering the analytical results provided for homogeneous macro-scale beams by GARCIA and VILLAÇA [58]. These results are reported in [1]. The homogeneous beam has the following properties:

$$(4.19) \quad E = 50 \text{ GPa}, \quad \rho = 2500 \text{ kg/m}^3, \quad \nu = 0.2,$$

$$(4.20) \quad L = 4 \text{ m}, \quad h = 0.6 \text{ m}, \quad b = 0.2 \text{ m}, \quad \kappa_s = 5.6.$$

The length scale parameter is taken as zero. Figure 4 presents the comparison of the time variation of mid-point deflection $w(L/2, t)$ of the homogeneous beam pinned at both ends computed by D-BEM to that evaluated by the analytical formula for different loading types. For distributed step loading in Fig. 4a, q_0 is taken as 100 kN/m. 16 cells are used in discretization, and time step is taken as 4×10^{-5} s. The developed method produces results with high degree of accuracy, which is evident from the excellent agreement between the two sets of results. Highly accurate results are also computed for concentrated harmonic loading as shown in Fig. 4b. The number of cells and the time step are the same as those used for distributed loading. The magnitude of the concentrated force is 2×10^5 N, and acts at $x_0 = L/2$ with a frequency of $\omega_P = 500$ Hz. A time response of the beam for the impulsive force with an amplitude of $P = 100$ N · s applied at $x_0 = L/2$ is

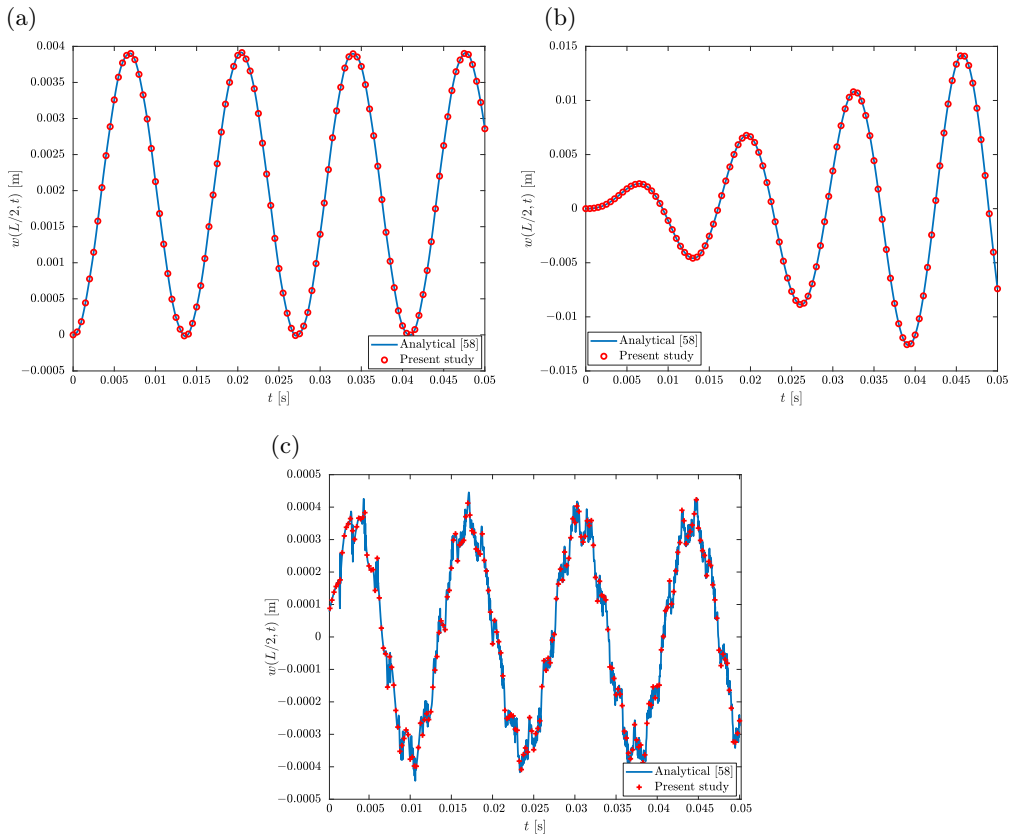


FIG. 4. Dynamic responses generated by D-BEM and the analytical formula for a pinned-pinned homogeneous beam under (a) distributed step loading with $q_0 = 100$ kN/m, (b) concentrated harmonic loading with $P = 0.2$ MN, $\omega_P = 500$ Hz, $x_0 = L/2$, and (c) impulsive loading with $P = 100$ N · s, $x_0 = L/2$.

depicted in Fig. 4c. In this case, a total of 64 cells are used, and time-step is set as 10^{-6} s. Again an excellent agreement is observed, which is indicative of the high level accuracy achieved by the application of the domain-boundary element method.

4.2. Parametric analyses

In this section, we present the numerical results generated for forced vibrations of functionally graded micro-beams with a variable length scale parameter. Dynamic loading functions are the same as those given by Eqs. (4.12)–(4.14). In all computations, the micro-beam is assumed to be pinned at both ends.

First, convergence characteristics of the developed technique are investigated. The variation of the mid-point deflection $w(L/2, t)$ of an FGM micro-beam, sub-

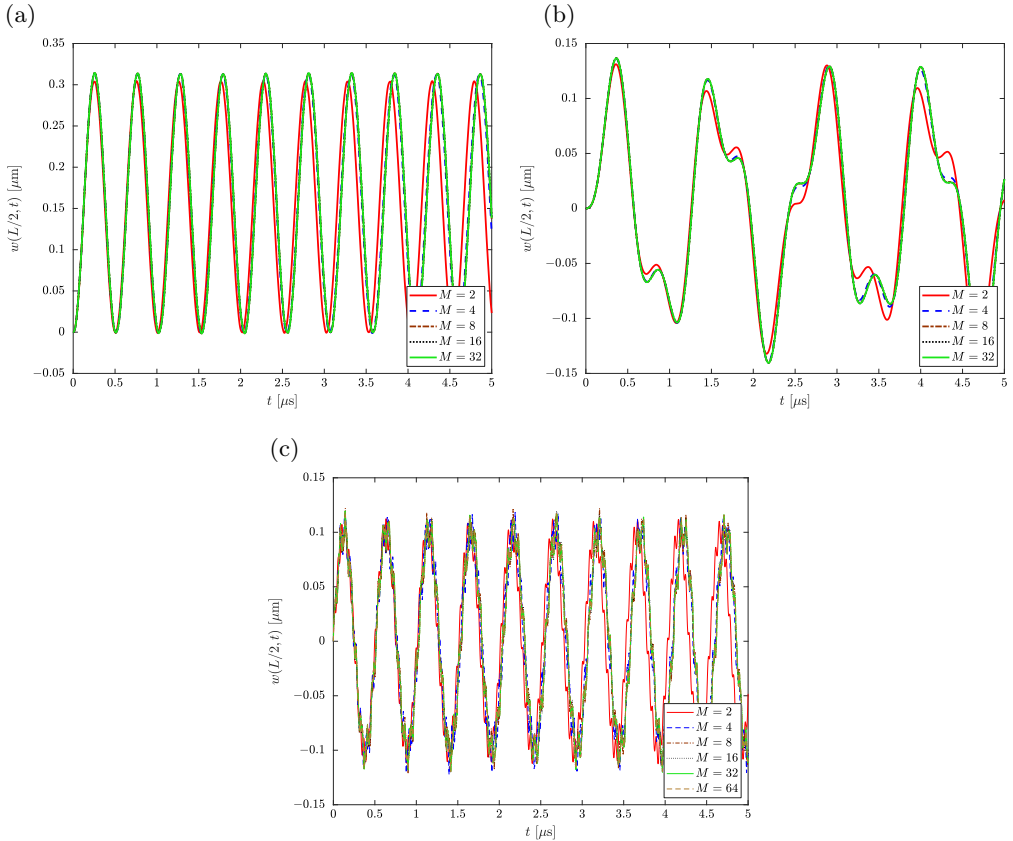


FIG. 5. Dynamic deflection of an FGM micro-beam with $\lambda = 0.5$, and $l_c/l_m = 1.0$ for different values of M and subjected to (a) distributed step loading with $q_0 = 100$ N/m, (b) concentrated harmonic loading with $P = 0.01$ N, $x_0 = L/2$, $\omega_P = 5$ MHz, and (c) impulsive loading with $P = 0.001$ $\mu\text{N} \cdot \text{s}$, $x_0 = L/2$.

jected to uniformly distributed step loading and concentrated harmonic loading are depicted in Figs. 5a and 5b, respectively. The results are generated by changing the total cell number M . Load intensities are taken as $q_0 = 1 \text{ kN/m}$, and $P = 0.01 \text{ N}$. Inhomogeneity exponent is $\lambda = 0.5$ and the length scale parameter ratio is set as $l_c/l_m = 1.0$. Rapid convergence is observed as the number of cells is increased from 2 to 16. For impulsive loading with an intensity of $P = 0.001 \mu\text{N} \cdot \text{s}$, the use of 64 cells assures the convergence as shown in Fig. 5c. Hence, in the parametric analyses presented in this section, number of cells employed in discretization is 16 for distributed and concentrated harmonic loads, and 64 for impulsive forcing.

The time step Δt has to be taken sufficiently small to assure a stable numerical solution procedure. Convergence studies conducted indicate that the time step should be taken as $1 \times 10^{-5} \text{ s}$ for distributed and harmonic loads, whereas for impulsive loading it should be equal to $1 \times 10^{-6} \text{ s}$.

Figures 6–8 depict the dynamic response of a functionally graded micro-beam for different values of the power-law index λ . The figures show the time histories of mid-point deflection $w(L/2, t)$ and normal stress $\sigma_{xx}(L/2, h/2, t)$. The functionally graded micro-beam is ceramic-rich when $\lambda < 1$, and metal-rich when $\lambda > 1$. Figure 6 presents deflection and stress for a micro-beam subjected to distributed step loading. Under this type of loading, both deflection and stress possess constant-amplitude harmonic variations. Forced vibration amplitudes increase and the vibration frequency decreases as λ gets larger. Figure 7 shows w and σ_{xx} variations for an FGM micro-beam subjected to a concentrated harmonic force. The vibration amplitude again gets larger as the inhomogeneity index λ is increased from 0.5 to 5. This is due to the drop in the micro-beam stiffness. Results pertaining to impulsive loading are provided in Fig. 8. Since impulsive

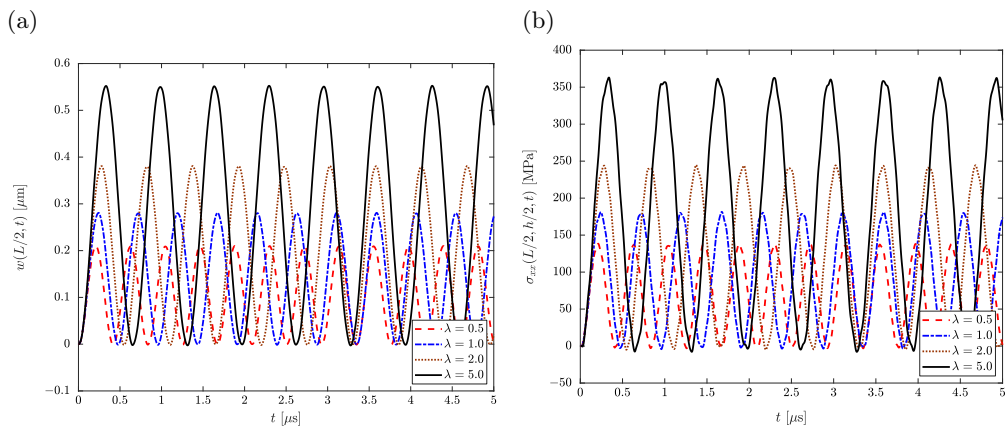


FIG. 6. Dynamic response of an FGM micro-beam under distributed step loading. $q_0 = 100 \text{ N/m}$, and $l_c/l_m = 3/2$.

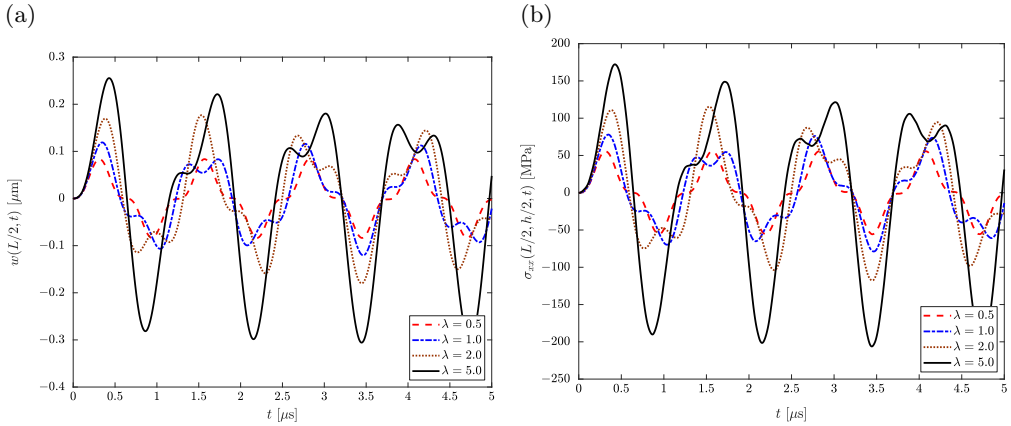


FIG. 7. Dynamic response of an FGM micro-beam under concentrated harmonic excitation. $P = 0.01 \text{ N}$, $\omega_P = 5 \text{ MHz}$, $x_0 = L/2$. and $l_c/l_m = 3/2$.

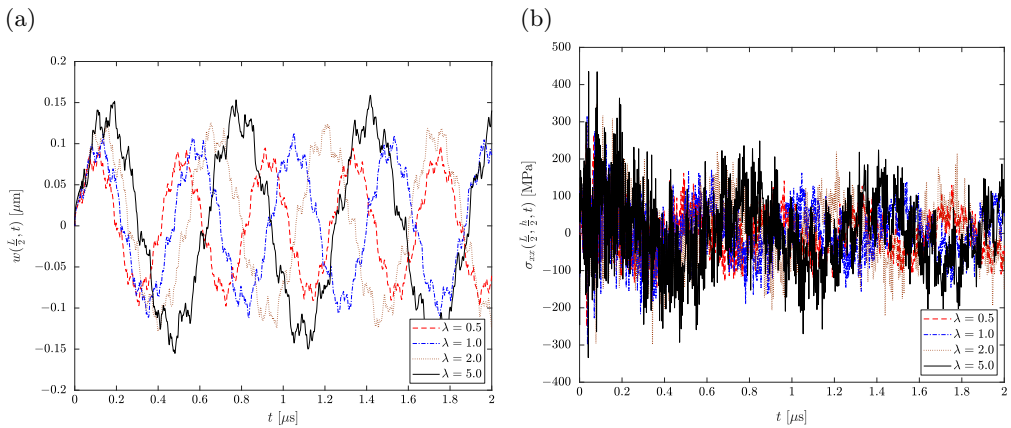


FIG. 8. Dynamic response of an FGM micro-beam subjected to impulsive loading. $P = 0.001 \mu\text{N} \cdot \text{s}$, $x_0 = L/2$, and $l_c/l_m = 3/2$.

loads have a wider range of frequencies, response functions are not as smooth as those generated for distributed and concentrated forces. Figure 8 indicates that compared to the vertical deflection w , normal stress σ_{xx} possesses higher frequency variations. This results from the dependence of σ_{xx} on derivatives $\partial u/\partial x$ and $\partial \varphi/\partial x$. Higher frequency behaviors of these derivatives cause the normal stress to follow a similar pattern.

The effect of length scale parameter ratio l_c/l_m on the deflection and stress of an FGM micro-beam is examined in Figs. 9–11. It is seen that an increase in l_c/l_m from $1/3$ to 2 causes a drop in the amplitude of forced vibrations and an increase in the response frequency. Thus, it can be concluded that the increase

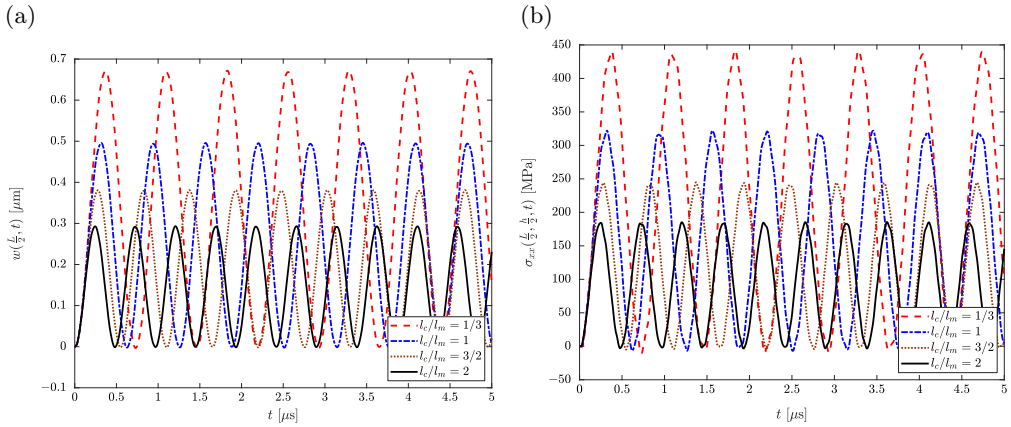


FIG. 9. Dynamic response of an FGM micro-beam under distributed step loading for different values of l_c/l_m . $q_0 = 100 \text{ N/m}$, and $\lambda = 2$.

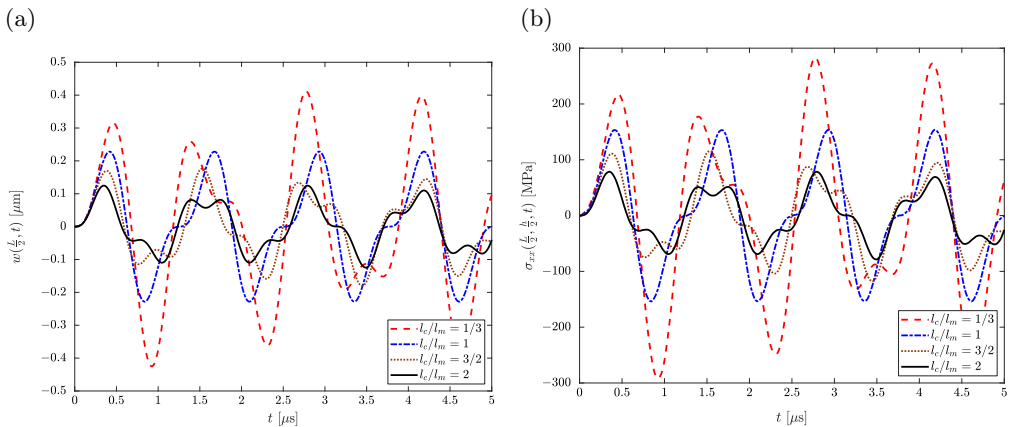


FIG. 10. Dynamic response of an FGM micro-beam under concentrated harmonic excitation for different values of l_c/l_m ; $P = 0.01 \text{ N}$, $\omega_P = 5 \text{ MHz}$, $x_0 = L/2$, and $\lambda = 2$.

in the length scale parameter ratio lowers deflection and stress levels in graded micro-beams. Again, since impulsive loads have a wider range of frequencies, response functions for this forcing type are not as smooth as those generated for distributed and concentrated forcings.

The effect of the length scale parameter ratio on the deviatoric part of the couple stress tensor is examined in Fig. 12. The figure shows that the increase in the length scale parameter ratio causes a corresponding increase in the amplitude of a couple stress component. Under all three loading conditions, the deviatoric part of the couple stress tensor for $l_c/l_m = 2$ is significantly larger than that calculated for $l_c/l_m = 1/3$. This is in contrast with the behavior observed for

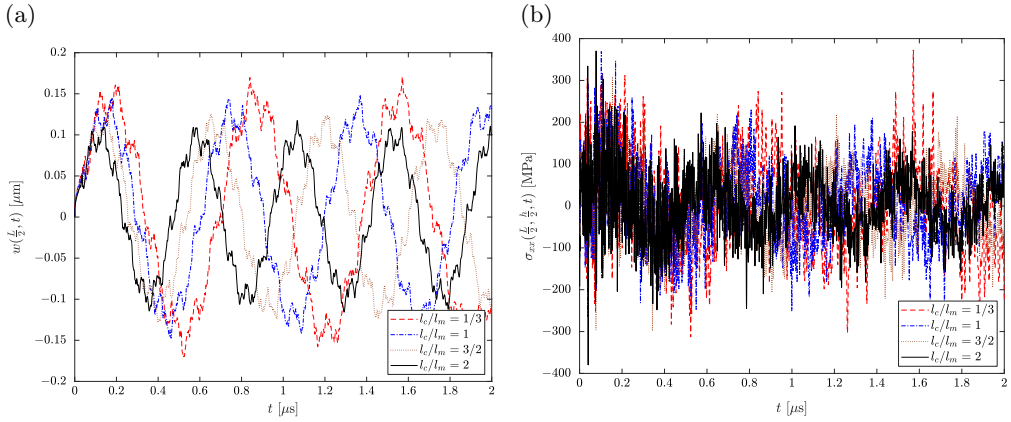


FIG. 11. Dynamic response of an FGM micro-beam subjected to impulsive loading for different values of l_c/l_m ; $P = 0.001 \mu\text{N} \cdot \text{s}$, $x_0 = L/2$, and $\lambda = 2$.

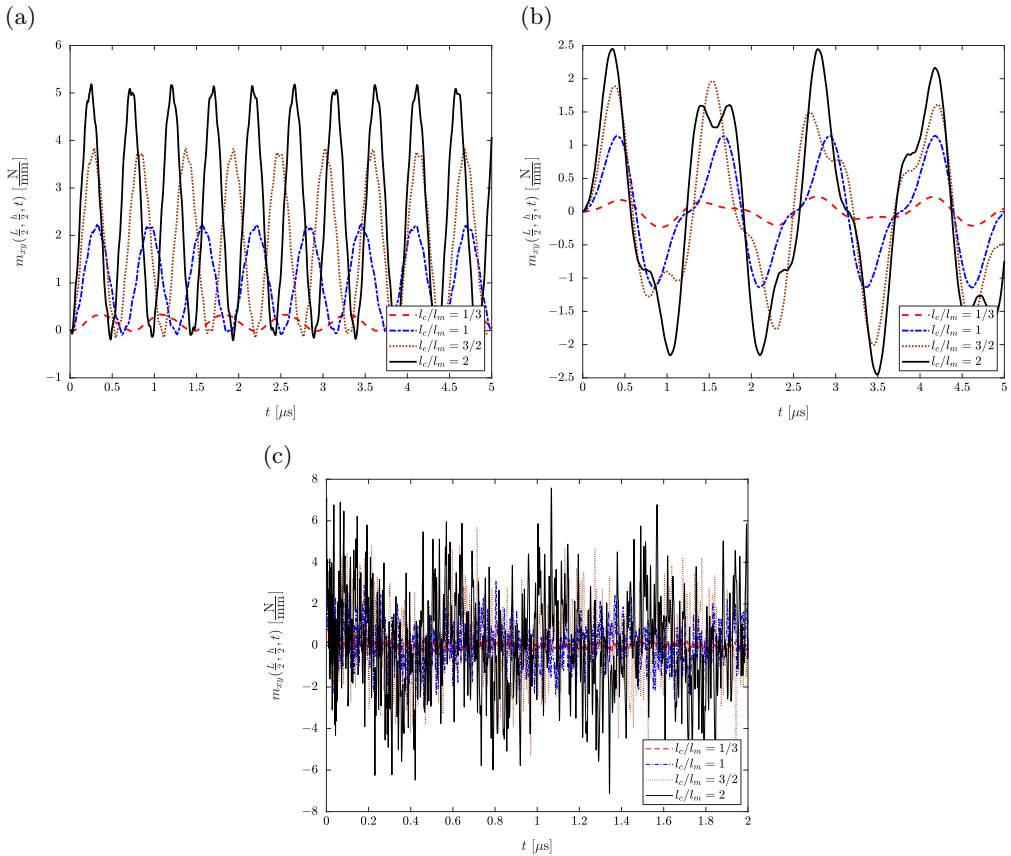


FIG. 12. Effect of length scale parameter ratio on m_{xy} for an FGM micro-beam with $\lambda = 2$, and under (a) distributed step loading with $q_0 = 100 \text{ N/m}$, (b) concentrated harmonic loading with $P = 0.01 \text{ N}$, $\omega_P = 5 \text{ MHz}$, $x_0 = L/2$, and (c) impulsive loading with $P = 0.001 \mu\text{N} \cdot \text{s}$, $x_0 = L/2$.

the normal stress σ_{xx} , which in general decreases significantly as the length scale parameter ratio is increased.

5. Concluding remarks

A domain-boundary element method is developed to examine transient dynamic behavior of functionally graded micro-beams. Small-scale effects are accounted for by applying the modified couple stress theory. Static fundamental solutions are used to express the weighted residual statements for the governing partial differential equations. The weighted residual statements are converted to a system of integral equations, which is reduced to a system of ordinary differential equations in time. The differential equation system is solved numerically by means of the Houbolt method. Presented numerical results illustrate the effects of material inhomogeneity and the length scale parameter ratio on the forced vibration behavior of FGM micro-beams.

Developed procedures are verified by comparisons to the results generated by analytical and numerical methods in the literature. Our results generated by D-BEM are shown to be in excellent agreement with those provided in the cited references. Thus, we conclude that the domain-boundary method is a reliable and accurate way of carrying out forced vibration analysis of micro-scale functionally graded beams. In addition to the verification study, convergence studies are performed to determine the number of cells to be used in domain discretization, and the time step to be applied in the numerical solution. A larger number of cells and a smaller time step is found to be required for dynamic analysis under impulsive loading.

Numerical results presented show that, as the power-law index λ is increased, displacement and normal stress amplitudes for an FGM micro-beam also increase. This implies that metal-rich beams undergo larger displacements, and are subjected to larger stresses. The functionally graded micro-beam vibrates with the frequency of applied load under harmonic excitation. An impulsive force, on the other hand, has a range of frequency, and this is reflected in time histories of displacements and stresses. The influence of the small-scale parameter l_c/l_m , which is named the length scale parameter ratio, is also examined. An increase in this parameter leads to smaller displacement and normal stress amplitudes. This trend is reversed for the deviatoric part of the couple stress tensor, i.e., increase in the l_c/l_m value results in a larger m_{xy} magnitude.

The method proposed in this study can be applied to solve static bending, and free and forced vibration problems involving functionally graded macro- and micro-scale beams. Shear deformation of the beam is considered by using the Timoshenko beam theory. Variations of all material properties including the length scale parameter are taken into account in the formulation. Thus, the

method will be particularly useful in design, analysis, and optimization studies involving graded micro-beams under transient dynamic effects. The presented procedure may also serve as the first step towards future developments regarding transient dynamic analysis of micro-scale plates and shells.

Appendix A. Matrix form of governing equations of motion

Equation (3.29) may be expressed as follows:

(A.1)

$$\begin{bmatrix}
 \mathbf{H}_{uu}^{bb} & 0 & 0 & \mathbf{H}_{u\varphi}^{bb} & 0 & 0 & 0 & 0 \\
 0 & \mathbf{H}_{ww}^{bb} & \mathbf{H}_{w,x}^{bb} & \mathbf{H}_{w\varphi}^{bb} + \mathbf{P}_{w\varphi}^{bb} & 0 & 0 & 0 & \mathbf{P}_{w,x\varphi}^{bd} \\
 0 & 0 & \mathbf{H}_{w,x,w}^{bb} & \mathbf{H}_{w,x\varphi}^{bb} + \mathbf{P}_{w,x\varphi}^{bb} & 0 & 0 & 0 & \mathbf{P}_{w,x\varphi}^{bd} \\
 \mathbf{H}_{\varphi u}^{bb} + \mathbf{P}_{\varphi u}^{bb} & \mathbf{H}_{\varphi w}^{bb} + \mathbf{P}_{\varphi w}^{bb} & \mathbf{H}_{\varphi w,x}^{bb} & \mathbf{H}_{\varphi\varphi}^{bb} & \mathbf{P}_{\varphi u}^{bd} & \mathbf{P}_{\varphi w}^{bd} & 0 & 0 \\
 \mathbf{H}_{uu}^{db} & 0 & 0 & \mathbf{H}_{u\varphi}^{db} & \mathbf{I} & 0 & 0 & \mathbf{H}_{u\varphi}^{dd} \\
 0 & \mathbf{H}_{ww}^{db} & \mathbf{H}_{w,x}^{db} & \mathbf{H}_{w\varphi}^{db} + \mathbf{P}_{w\varphi}^{db} & 0 & \mathbf{I} & 0 & \mathbf{P}_{w\varphi}^{dd} \\
 0 & 0 & \mathbf{H}_{w,x,w}^{db} & \mathbf{H}_{w,x\varphi}^{db} + \mathbf{P}_{w,x\varphi}^{db} & 0 & 0 & \mathbf{I} & \mathbf{I} + \mathbf{P}_{w,x\varphi}^{dd} \\
 \mathbf{H}_{\varphi u}^{db} + \mathbf{P}_{\varphi u}^{db} & \mathbf{H}_{\varphi w}^{db} + \mathbf{P}_{\varphi w}^{db} & \mathbf{H}_{\varphi w,x}^{db} & \mathbf{H}_{\varphi\varphi}^{db} & \mathbf{H}_{\varphi u}^{dd} + \mathbf{P}_{\varphi u}^{dd} & \mathbf{P}_{\varphi w}^{dd} & \mathbf{H}_{\varphi w,x}^{dd} & \mathbf{I}
 \end{bmatrix}
 \begin{Bmatrix}
 \mathbf{u}^b \\
 \mathbf{w}^b \\
 \mathbf{w}_{,x}^b \\
 \varphi^b \\
 \mathbf{u}^d \\
 \mathbf{w}^d \\
 \mathbf{w}_{,x}^d \\
 \varphi^d
 \end{Bmatrix}$$

$$=
 \begin{bmatrix}
 \mathbf{S}_{uu}^{bb} & 0 & 0 & \mathbf{S}_{u\varphi}^{bb} & \mathbf{S}_{uu}^{bd} & 0 & 0 & \mathbf{S}_{u\varphi}^{bd} \\
 0 & \mathbf{S}_{ww}^{bb} & 0 & 0 & 0 & \mathbf{S}_{ww}^{bd} & 0 & 0 \\
 0 & \mathbf{S}_{w,xw}^{bb} & 0 & 0 & 0 & \mathbf{S}_{w,xw}^{bd} & 0 & 0 \\
 \mathbf{S}_{\varphi u}^{bb} & 0 & 0 & \mathbf{S}_{\varphi\varphi}^{bb} & \mathbf{S}_{\varphi u}^{bd} & 0 & 0 & \mathbf{S}_{\varphi\varphi}^{bd} \\
 \mathbf{S}_{uu}^{db} & 0 & 0 & \mathbf{S}_{u\varphi}^{db} & \mathbf{S}_{uu}^{dd} & 0 & 0 & \mathbf{S}_{u\varphi}^{dd} \\
 0 & \mathbf{S}_{ww}^{db} & 0 & 0 & 0 & \mathbf{S}_{ww}^{dd} & 0 & 0 \\
 0 & \mathbf{S}_{w,xw}^{db} & 0 & 0 & 0 & \mathbf{S}_{w,xw}^{dd} & 0 & 0 \\
 \mathbf{S}_{\varphi u}^{db} & 0 & 0 & \mathbf{S}_{\varphi\varphi}^{db} & \mathbf{S}_{\varphi u}^{dd} & 0 & 0 & \mathbf{S}_{\varphi\varphi}^{dd}
 \end{bmatrix}
 \begin{Bmatrix}
 \ddot{\mathbf{u}}^b \\
 \ddot{\mathbf{w}}^b \\
 \ddot{\mathbf{w}}_{,x}^b \\
 \ddot{\varphi}^b \\
 \ddot{\mathbf{u}}^d \\
 \ddot{\mathbf{w}}^d \\
 \ddot{\mathbf{w}}_{,x}^d \\
 \ddot{\varphi}^d
 \end{Bmatrix}$$

$$+
 \begin{bmatrix}
 \mathbf{G}_{uu}^{bb} & 0 & 0 & 0 \\
 0 & \mathbf{G}_{ww}^{bb} & \mathbf{G}_{w,x}^{bb} & 0 \\
 0 & \mathbf{G}_{w,xw}^{bb} & \mathbf{G}_{w,x,w}^{bb} & 0 \\
 0 & 0 & 0 & \mathbf{G}_{\varphi\varphi}^{bb} \\
 \mathbf{G}_{uu}^{db} & 0 & 0 & 0 \\
 0 & \mathbf{G}_{ww}^{db} & \mathbf{G}_{w,x}^{db} & 0 \\
 0 & \mathbf{G}_{w,xw}^{db} & \mathbf{G}_{w,x,w}^{db} & 0 \\
 0 & 0 & 0 & \mathbf{G}_{\varphi\varphi}^{db}
 \end{bmatrix}
 \begin{Bmatrix}
 \mathbf{N}^b \\
 \mathbf{Q}^b \\
 \mathbf{R}^b \\
 \mathbf{M}^b
 \end{Bmatrix}
 +
 \begin{Bmatrix}
 0 \\
 \mathbf{f}^b \\
 \mathbf{m}^b \\
 0 \\
 0 \\
 \mathbf{f}^d \\
 \mathbf{m}^d \\
 0
 \end{Bmatrix}.$$

The superscripts b and d respectively stand for boundary and domain. Thus, \mathbf{u}^b , \mathbf{w}^b , $\mathbf{w}_{,x}^b$, and φ^b are generalized displacements of boundary nodes; and \mathbf{u}^d , \mathbf{w}^d , $\mathbf{w}_{,x}^d$, and φ^d are generalized displacements of internal nodes. \mathbf{N}^b , \mathbf{Q}^b , \mathbf{R}^b , and \mathbf{M}^b are respectively axial force, shear force, and bending moment vectors

at the boundary nodes. The vectors \mathbf{f}^b , \mathbf{m}^b , and \mathbf{f}^d , \mathbf{m}^d are nodal external load vectors. The sub-matrices computed at the boundary are defined as given below:

$$(A.2) \quad \mathbf{H}_{uu}^{bb} = \frac{1}{2} \begin{bmatrix} 1 & -1 \\ -1 & 1 \end{bmatrix},$$

$$(A.3) \quad \mathbf{H}_{u\varphi}^{bb} = \frac{B_{11}}{2A_{11}} \begin{bmatrix} -1 & 1 \\ 1 & -1 \end{bmatrix},$$

$$(A.4) \quad \mathbf{H}_{ww}^{bb} = \frac{1}{2} \begin{bmatrix} 1 & -1 \\ -1 & 1 \end{bmatrix},$$

$$(A.5) \quad \mathbf{H}_{w,xw,x}^{bb} = \frac{1}{2} \begin{bmatrix} 1 & -\cosh[\sqrt{\Lambda_w} L] \\ -\cosh[\sqrt{\Lambda_w} L] & 1 \end{bmatrix},$$

$$(A.6) \quad \mathbf{H}_{w,x\varphi}^{bb} = \frac{1}{2} \begin{bmatrix} 1 & -\cosh[\sqrt{\Lambda_w} L] \\ -\cosh[\sqrt{\Lambda_w} L] & 1 \end{bmatrix},$$

$$(A.7) \quad \mathbf{H}_{\varphi u}^{bb} = \frac{B_{11}}{2(D_{11} + A_{552}/4)} \begin{bmatrix} -1 & \cosh(\sqrt{\Lambda_\varphi} L) \\ \cosh(\sqrt{\Lambda_\varphi} L) & -1 \end{bmatrix},$$

$$(A.8) \quad \mathbf{H}_{\varphi w}^{bb} = \frac{\sqrt{\Lambda_\varphi} \sinh(\sqrt{\Lambda_\varphi} L)}{2} \left(1 + \frac{A_{552}/4}{D_{11} + A_{552}/4} \right) \begin{bmatrix} 0 & 1 \\ -1 & 0 \end{bmatrix},$$

$$(A.9) \quad \mathbf{H}_{\varphi w,x}^{bb} = \frac{\sqrt{\Lambda_\varphi} \sinh(\sqrt{\Lambda_\varphi} L)}{2} \begin{bmatrix} 0 & 1 \\ -1 & 0 \end{bmatrix},$$

$$(A.10) \quad \mathbf{H}_{\varphi\varphi}^{bb} = \frac{1}{2} \begin{bmatrix} 1 & -\cosh(\sqrt{\Lambda_\varphi} L) \\ -\cosh(\sqrt{\Lambda_\varphi} L) & 1 \end{bmatrix},$$

$$(A.11) \quad \mathbf{G}_{uu}^{bb} = \frac{L}{2A_{11}} \begin{bmatrix} 0 & 1 \\ -1 & 0 \end{bmatrix},$$

$$(A.12) \quad \mathbf{G}_{ww}^{bb} = \frac{1}{\kappa_s F_{55}} \left[\frac{L}{2} - \frac{\sinh(\sqrt{\Lambda_w} L)}{2\sqrt{\Lambda_w}} \right] \begin{bmatrix} 0 & 1 \\ -1 & 0 \end{bmatrix},$$

$$(A.13) \quad \mathbf{G}_{ww,x}^{bb} = \frac{1 - \cosh(\sqrt{\Lambda_w} L)}{2\kappa_s F_{55}} \begin{bmatrix} 0 & 1 \\ 1 & 0 \end{bmatrix},$$

$$(A.14) \quad \mathbf{G}_{w,xw}^{bb} = -\frac{1}{\kappa_s F_{55}} \left[\frac{1}{2} - \frac{\cosh(\sqrt{\Lambda_w} L)}{2} \right] \begin{bmatrix} 0 & 1 \\ 1 & 0 \end{bmatrix},$$

$$(A.15) \quad \mathbf{G}_{w,xw,x}^{bb} = \frac{\sqrt{\Lambda_w} \sinh(\sqrt{\Lambda_w} L)}{2\kappa_s F_{55}} \begin{bmatrix} 0 & 1 \\ -1 & 0 \end{bmatrix},$$

$$(A.16) \quad \mathbf{G}_{\varphi\varphi}^{bb} = \frac{\sinh(\sqrt{\Lambda_\varphi} L)}{2\sqrt{\Lambda_\varphi} (D_{11} + A_{552}/4)} \begin{bmatrix} 0 & 1 \\ -1 & 0 \end{bmatrix}.$$

Domain dependent sub-matrices that do not involve domain integrals are of the forms:

$$(A.17) \quad \mathbf{H}_{uu}^{db} = -\frac{1}{2}[1 \ 1],$$

$$(A.18) \quad \mathbf{H}_{u\varphi}^{db} = \frac{B_{11}}{2A_{11}}[1 \ 1],$$

$$(A.19) \quad \mathbf{H}_{u\varphi}^{dd} = -\frac{B_{11}}{A_{11}}\mathbf{I},$$

$$(A.20) \quad \mathbf{H}_{ww}^{db} = -\frac{1}{2}[1 \ 1],$$

$$(A.21) \quad \mathbf{H}_{w,x}^{db} = \frac{1}{2\sqrt{\Lambda_w}}[-\sinh[\sqrt{\Lambda_w}\xi_k] \ \sinh[\sqrt{\Lambda_w}(L-\xi_k)]],$$

$$(A.22) \quad \mathbf{H}_{w\varphi}^{db} = \frac{1}{2\sqrt{\Lambda_w}}[-\sinh[\sqrt{\Lambda_w}\xi_k] \ \sinh[\sqrt{\Lambda_w}(L-\xi_k)]],$$

$$(A.23) \quad \mathbf{H}_{w,xw,x}^{db} = -\frac{1}{2}[\cosh[\sqrt{\Lambda_w}\xi_k] \ \cosh[\sqrt{\Lambda_w}(L-\xi_k)]],$$

$$(A.24) \quad \mathbf{H}_{w,x\varphi}^{db} = -\frac{1}{2}[\cosh[\sqrt{\Lambda_w}\xi_k] \ \cosh[\sqrt{\Lambda_w}(L-\xi_k)]],$$

$$(A.25) \quad \mathbf{H}_{\varphi u}^{db} = \frac{B_{11}}{2(D_{11}+A_{552}/4)}[\cosh(\sqrt{\Lambda_\varphi}\xi_k) \ \cosh[\sqrt{\Lambda_\varphi}(L-\xi_k)]],$$

$$(A.26) \quad \mathbf{H}_{\varphi w}^{db} = \frac{\sqrt{\Lambda_\varphi}}{2}\left(1 + \frac{A_{552}/4}{D_{11}+A_{552}/4}\right) \\ \times [-\sinh(\sqrt{\Lambda_\varphi}\xi_k) \ \sinh[\sqrt{\Lambda_\varphi}(L-\xi_k)]],$$

$$(A.27) \quad \mathbf{H}_{\varphi w,x}^{db} = -\frac{A_{552}/4}{2(D_{11}+A_{552}/4)}[\cosh(\sqrt{\Lambda_\varphi}\xi_k) \ \cosh[\sqrt{\Lambda_\varphi}(L-\xi_k)]],$$

$$(A.28) \quad \mathbf{H}_{\varphi\varphi}^{db} = -\frac{1}{2}[\cosh(\sqrt{\Lambda_\varphi}\xi_k) \ \cosh[\sqrt{\Lambda_\varphi}(L-\xi_k)]],$$

$$(A.29) \quad \mathbf{H}_{\varphi u}^{dd} = -\frac{B_{11}}{D_{11}+A_{552}/4}\mathbf{I},$$

$$(A.30) \quad \mathbf{H}_{\varphi w,x}^{dd} = \frac{A_{552}/4}{D_{11}+A_{552}/4}\mathbf{I},$$

$$(A.31) \quad \mathbf{G}_{uu}^{db} = \frac{1}{2A_{11}}[-\xi_k \ (L-\xi_k)],$$

$$(A.32) \quad \mathbf{G}_{ww}^{db} = \frac{1}{2\kappa_s F_{55}} \\ \times \left[-\left(\xi_k - \frac{\sinh[\sqrt{\Lambda_w}\xi_k]}{\sqrt{\Lambda_w}}\right) \left((L-\xi_k) - \frac{\sinh[\sqrt{\Lambda_w}(L-\xi_k)]}{\sqrt{\Lambda_w}} \right) \right],$$

$$(A.33) \quad \mathbf{G}_{ww,x}^{db} = \frac{1}{2\kappa_s F_{55}}[(1-\cosh[\sqrt{\Lambda_w}\xi_k]) \ (1-\cosh[\sqrt{\Lambda_w}(L-\xi_k)])],$$

$$(A.34) \quad \mathbf{G}_{w,xw}^{db} = \frac{1}{2\kappa_s F_{55}}[(1-\cosh[\sqrt{\Lambda_w}\xi_k]) \ -(1-\cosh[\sqrt{\Lambda_w}(L-\xi_k)])],$$

$$(A.35) \quad \mathbf{G}_{w,xw,x}^{db} = \frac{\sqrt{\Lambda_w}}{2\kappa_s F_{55}} [-\sinh[\sqrt{\Lambda_w} \xi_k] \quad \sinh[\sqrt{\Lambda_w} (L-\xi_k)]],$$

$$(A.36) \quad \mathbf{G}_{\varphi\varphi}^{db} = \frac{1}{2\sqrt{\Lambda_\varphi}(D_{11}+A_{552}/4)} [-\sinh[\sqrt{\Lambda_\varphi} \xi_k] \quad \sinh[\sqrt{\Lambda_\varphi} (L-\xi_k)]],$$

where \mathbf{I} is the identity matrix of size $(N - 2) \times (N - 2)$.

Appendix B. Domain-dependent sub-matrices

The domain integrals in Eqs. (3.20)–(3.23) are needed in the construction of submatrices \mathbf{S} and \mathbf{P} in Eq. (A.1). Utilizing Eqs. (3.4)–(3.6) and (3.24)–(3.26), these domain integrals are expressed as:

$$(B.1) \quad \int_{x_1^j}^{x_3^j} \frac{|x - \xi_k|}{2} \zeta(x, t) dx = [m_1^{kj} \quad m_2^{kj} \quad m_3^{kj}] \begin{Bmatrix} \zeta_1^j \\ \zeta_2^j \\ \zeta_3^j \end{Bmatrix},$$

$$(B.2) \quad \int_{x_1^j}^{x_3^j} \frac{\text{sgn}(x - \xi_k)}{2} \zeta(x, t) dx = [p_1^{kj} \quad p_2^{kj} \quad p_3^{kj}] \begin{Bmatrix} \zeta_1^j \\ \zeta_2^j \\ \zeta_3^j \end{Bmatrix},$$

$$(B.3) \quad \int_{x_1^j}^{x_3^j} \frac{\text{sgn}(x - \xi_k)}{2} \cosh(\sqrt{\Lambda} |x - \xi_k|) \zeta(x, t) dx = [\bar{p}_1^{kj} \quad \bar{p}_2^{kj} \quad \bar{p}_3^{kj}] \begin{Bmatrix} \zeta_1^j \\ \zeta_2^j \\ \zeta_3^j \end{Bmatrix},$$

$$(B.4) \quad \int_{x_1^j}^{x_3^j} \frac{\sinh(\sqrt{\Lambda} |x - \xi_k|)}{2\sqrt{\Lambda}} \zeta(x, t) dx = [\bar{m}_1^{kj} \quad \bar{m}_2^{kj} \quad \bar{m}_3^{kj}] \begin{Bmatrix} \zeta_1^j \\ \zeta_2^j \\ \zeta_3^j \end{Bmatrix},$$

where $\zeta(x, t)$ could be unknown displacement functions or their second time derivative and ζ_i^j is the value of ζ at the i^{th} node of the j^{th} cell at time t . Note that Λ in Eqs. (B.3) and (B.4) takes the values of Λ_w or Λ_φ depending on the domain integral being evaluated.

There are three possibilities regarding the relative position of the source node ξ_k with respect to the element $\Omega_j = [x_1^j, x_3^j]$. These are $\xi_k \leq x_1^j$; $\xi_k \equiv x_2^j$; and $\xi_k \geq x_3^j$. For $\xi_k \leq x_1^j$, we get the following expressions:

$$(B.5) \quad m_1^{kj} = \frac{(x_1^j - \xi_k)h_c}{6}, \quad m_2^{kj} = \frac{2(x_2^j - \xi_k)h_c}{3}, \quad m_3^{kj} = \frac{(x_3^j - \xi_k)h_c}{6},$$

$$(B.6) \quad p_1^{kj} = \frac{h_c}{6}, \quad p_2^{kj} = \frac{2h_c}{3}, \quad p_3^{kj} = \frac{h_c}{6},$$

$$(B.7) \quad \bar{p}_1^{kj} = \frac{1}{4\Lambda^{3/2}h_c^2} \left\{ 2 \sinh[\sqrt{\Lambda}(x_3^j - \xi_k)] - 2(1 + \Lambda h_c^2) \sinh[\sqrt{\Lambda}(x_1^j - \xi_k)] \right. \\ \left. - \sqrt{\Lambda}h_c \{ 3 \cosh[\sqrt{\Lambda}(x_1^j - \xi_k)] + \cosh[\sqrt{\Lambda}(x_3^j - \xi_k)] \} \right\},$$

$$(B.8) \quad \bar{p}_2^{kj} = \frac{1}{\Lambda^{3/2}h_c^2} \left\{ \sinh[\sqrt{\Lambda}(x_1^j - \xi_k)] - \sinh[\sqrt{\Lambda}(x_3^j - \xi_k)] \right. \\ \left. + \sqrt{\Lambda}h_c \{ \cosh[\sqrt{\Lambda}(x_1^j - \xi_k)] + \cosh[\sqrt{\Lambda}(x_3^j - \xi_k)] \} \right\},$$

$$(B.9) \quad \bar{p}_3^{kj} = \frac{1}{4\Lambda^{3/2}h_c^2} \left\{ 2(1 + \Lambda h_c^2) \sinh[\sqrt{\Lambda}(x_3^j - \xi_k)] - 2 \sinh[\sqrt{\Lambda}(x_1^j - \xi_k)] \right. \\ \left. - \sqrt{\Lambda}h_c \{ \cosh[\sqrt{\Lambda}(x_1^j - \xi_k)] + 3 \cosh[\sqrt{\Lambda}(x_3^j - \xi_k)] \} \right\},$$

$$(B.10) \quad \bar{m}_1^{kj} = \frac{1}{4\Lambda^2h_c^2} \left\{ 2 \cosh[\sqrt{\Lambda}(x_3^j - \xi_k)] - 2(1 + \Lambda h_c^2) \cosh[\sqrt{\Lambda}(x_1^j - \xi_k)] \right. \\ \left. - \sqrt{\Lambda}h_c \{ 3 \sinh[\sqrt{\Lambda}(x_1^j - \xi_k)] + \sinh[\sqrt{\Lambda}(x_3^j - \xi_k)] \} \right\},$$

$$(B.11) \quad \bar{m}_2^{kj} = \frac{1}{\Lambda^2h_c^2} \left\{ \cosh[\sqrt{\Lambda}(x_1^j - \xi_k)] - \cosh[\sqrt{\Lambda}(x_3^j - \xi_k)] \right. \\ \left. + \sqrt{\Lambda}h_c \{ \sinh[\sqrt{\Lambda}(x_1^j - \xi_k)] + \sinh[\sqrt{\Lambda}(x_3^j - \xi_k)] \} \right\},$$

$$(B.12) \quad \bar{m}_3^{kj} = \frac{1}{4\Lambda^2h_c^2} \left\{ 2(1 + \Lambda h_c^2) \cosh[\sqrt{\Lambda}(x_3^j - \xi_k)] - 2 \cosh[\sqrt{\Lambda}(x_1^j - \xi_k)] \right. \\ \left. - \sqrt{\Lambda}h_c \{ \sinh[\sqrt{\Lambda}(x_1^j - \xi_k)] + 3 \sinh[\sqrt{\Lambda}(x_3^j - \xi_k)] \} \right\}.$$

For the case of $\xi_k \equiv x_2^j$, we obtain:

$$(B.13) \quad m_1^{kj} = \frac{h_c^2}{8}, \quad m_2^{kj} = \frac{h_c^2}{4}, \quad m_3^{kj} = \frac{h_c^2}{8},$$

$$(B.14) \quad p_1^{kj} = -\frac{h_c}{4}, \quad p_2^{kj} = 0, \quad p_3^{kj} = \frac{h_c}{4},$$

$$(B.15) \quad \bar{p}_1^{kj} = \frac{1}{2\Lambda h_c} \left[\cosh(\sqrt{\Lambda}h_c) - \sqrt{\Lambda}h_c \sinh(\sqrt{\Lambda}h_c) - 1 \right],$$

$$(B.16) \quad \bar{p}_2^{kj} = 0,$$

$$(B.17) \quad \bar{p}_3^{kj} = \frac{1}{2\Lambda h_c} \left[\sqrt{\Lambda}h_c \sinh(\sqrt{\Lambda}h_c) - \cosh(\sqrt{\Lambda}h_c) + 1 \right],$$

$$(B.18) \quad \bar{m}_1^{kj} = \frac{1}{2\Lambda^2h_c^2} \left\{ (2 + \Lambda h_c^2) \cosh(\sqrt{\Lambda}h_c) - 2[1 + \sqrt{\Lambda}h_c \sinh(\sqrt{\Lambda}h_c)] \right\},$$

$$(B.19) \quad \bar{m}_2^{kj} = \frac{1}{\Lambda^2h_c^2} \left\{ 2[1 - \cosh(\sqrt{\Lambda}h_c) + \sqrt{\Lambda}h_c \sinh(\sqrt{\Lambda}h_c)] - \Lambda h_c^2 \right\},$$

$$(B.20) \quad \bar{m}_3^{kj} = \frac{1}{2\Lambda^2 h_c^2} \left\{ (2 + \Lambda h_c^2) \cosh(\sqrt{\Lambda} h_c) - 2[1 + \sqrt{\Lambda} h_c \sinh(\sqrt{\Lambda} h_c)] \right\}.$$

Expressions valid for $\xi_k \geq x_3^j$ are negatives of those found for $\xi_k \leq x_1^j$.

Appendix C. Load vectors

Three different types of loading are considered in parametric analyses, which are distributed step, concentrated harmonic, and concentrated impulsive loads. For uniformly distributed loading with intensity q , load vectors are given by:

$$(C.1) \quad \mathbf{f}^b = -\frac{q\left(\frac{L^2}{2} + \frac{1}{\Lambda_w} [1 - \cosh(\sqrt{\Lambda_w} L)]\right)}{2\kappa_s F_{55}} \begin{Bmatrix} 1 \\ 1 \end{Bmatrix},$$

$$(C.2) \quad \mathbf{f}^d = -\frac{q}{2\kappa_s F_{55}} \times \begin{Bmatrix} \frac{\xi_2^2 + (L - \xi_2)^2}{2} + \frac{1}{\Lambda_w} \{2 - \cosh[\sqrt{\Lambda_w}(L - \xi_2)] - \cosh[\sqrt{\Lambda_w} \xi_2]\} \\ \frac{\xi_3^2 + (L - \xi_3)^2}{2} + \frac{1}{\Lambda_w} \{2 - \cosh[\sqrt{\Lambda_w}(L - \xi_3)] - \cosh[\sqrt{\Lambda_w} \xi_3]\} \\ \vdots \\ \frac{\xi_{N-1}^2 + (L - \xi_{N-1})^2}{2} + \frac{1}{\Lambda_w} \{2 - \cosh[\sqrt{\Lambda_w}(L - \xi_{N-1})] - \cosh[\sqrt{\Lambda_w} \xi_{N-1}]\} \end{Bmatrix},$$

$$(C.3) \quad \mathbf{m}^b = -\frac{q(-L + \frac{1}{\sqrt{\Lambda_w}} \sinh(\sqrt{\Lambda_w} L))}{2\kappa_s F_{55}} \begin{Bmatrix} 1 \\ -1 \end{Bmatrix},$$

$$(C.4) \quad \mathbf{m}^d = -\frac{q}{2\kappa_s F_{55}} \times \begin{Bmatrix} 2\xi_2 - L + \frac{1}{\sqrt{\Lambda_w}} \left\{ \sinh[\sqrt{\Lambda_w}(L - \xi_2)] - \sinh[\sqrt{\Lambda_w} \xi_2] \right\} \\ 2\xi_3 - L + \frac{1}{\sqrt{\Lambda_w}} \left\{ \sinh[\sqrt{\Lambda_w}(L - \xi_3)] - \sinh[\sqrt{\Lambda_w} \xi_3] \right\} \\ \vdots \\ 2\xi_{N-1} - L + \frac{1}{\sqrt{\Lambda_w}} \left\{ \sinh[\sqrt{\Lambda_w}(L - \xi_{N-1})] - \sinh[\sqrt{\Lambda_w} \xi_{N-1}] \right\} \end{Bmatrix}.$$

For a concentrated force P applied at $x = x_0$, the vectors are written as:

$$(C.5) \quad \mathbf{f}^b = -\frac{P}{2\kappa_s F_{55}} \begin{Bmatrix} x_0 - \frac{1}{\sqrt{\Lambda_w}} \sinh(\sqrt{\Lambda_w} x_0) \\ L - x_0 - \frac{1}{\sqrt{\Lambda_w}} \sinh[\sqrt{\Lambda_w}(L - x_0)] \end{Bmatrix},$$

$$(C.6) \quad \mathbf{f}^d = -\frac{P}{2\kappa_s F_{55}} \begin{Bmatrix} |\xi_2 - x_0| - \frac{1}{\sqrt{\Lambda_w}} \sinh[\sqrt{\Lambda_w} |\xi_2 - x_0|] \\ |\xi_3 - x_0| - \frac{1}{\sqrt{\Lambda_w}} \sinh[\sqrt{\Lambda_w} |\xi_3 - x_0|] \\ \vdots \\ |\xi_{N-1} - x_0| - \frac{1}{\sqrt{\Lambda_w}} \sinh[\sqrt{\Lambda_w} |\xi_{N-1} - x_0|] \end{Bmatrix},$$

$$(C.7) \quad \mathbf{m}^b = -\frac{P}{2\kappa_s F_{55}} \left\{ \begin{array}{l} 1 - \cosh(\sqrt{\Lambda_w} x_0) \\ -1 + \cosh[\sqrt{\Lambda_w}(L - x_0)] \end{array} \right\},$$

$$(C.8) \quad \mathbf{m}^d = -\frac{P}{2\kappa_s F_{55}} \left\{ \begin{array}{l} \operatorname{sgn}(\xi_2 - x_0)\{-1 + \cosh[\sqrt{\Lambda_w} |\xi_2 - x_0|]\} \\ \operatorname{sgn}(\xi_3 - x_0)\{-1 + \cosh[\sqrt{\Lambda_w} |\xi_3 - x_0|]\} \\ \vdots \\ \operatorname{sgn}(\xi_{N-1} - x_0)\{-1 + \cosh[\sqrt{\Lambda_w} |\xi_{N-1} - x_0|]\} \end{array} \right\}.$$

References

1. J.A.M. CARRER, S.A. FLEISCHFRESSER, L.F.T. GARCIA, W.J. MANSUR, *Dynamic analysis of Timoshenko beams by the boundary element method*, Engineering Analysis with Boundary Elements, **37**, 12, 1602–1616, 2013.
2. I. ESHRAGHI, S. DAG, *Domain-boundary element method for elastodynamics of functionally graded Timoshenko beams*, Computers & Structures, **195**, 113–125, 2018.
3. Z. AHMED, I. ESHRAGHI, S. DAG, *Domain-boundary element method for forced vibrations of fiber-reinforced laminated beams*, International Journal of Computational Methods in Engineering Science and Mechanics, **21**, 3, 141–158, 2020.
4. J.A.M. CARRER, W.J. MANSUR, *Scalar wave equation by the boundary element method: A D-BEM approach with constant time-weighting functions*, International Journal for Numerical Methods in Engineering, **81**, 10, 1281–1297, 2010.
5. J.A.M. CARRER, W.J. MANSUR, R.J. VANZUIT, *Scalar wave equation by the boundary element method: a D-BEM approach with non-homogeneous initial conditions*, Computational Mechanics, **44**, 1, 31–44, 2009.
6. I. ESHRAGHI, S. DAG, *Forced vibrations of functionally graded annular and circular plates by domain-boundary element method*, ZAMM – Journal of Applied Mathematics and Mechanics/Zeitschrift für Angewandte Mathematik und Mechanik, **100**, 8, e201900048, 2020.
7. C.P. PROVIDAKIS, *Transient dynamic response of elastoplastic thick plates resting on Winkler-type foundation*, Nonlinear Dynamics, **23**, 3, 285–302, 2000.
8. G.D. HATZIGEORGIOU, D.E. BESKOS, *Dynamic elastoplastic analysis of 3-D structures by the domain/boundary element method*, Computers & Structures, **80**, 3–4, 339–347, 2002.
9. C.P. PROVIDAKIS, D.E. BESKOS, *Dynamic analysis of elasto-plastic flexural plates by the D/BEM*, Engineering Analysis with Boundary Elements, **14**, 1, 75–80, 1994.
10. D. SOARES, J.A.M. CARRER, W.J. MANSUR, *Non-linear elastodynamic analysis by the BEM: an approach based on the iterative coupling of the D-BEM and TD-BEM formulations*, Engineering Analysis with Boundary Elements, **29**, 8, 761–774, 2005.
11. R. PETTRES, L.A. DE LACERDA, J.A.M. CARRER, *A boundary element formulation for the heat equation with dissipative and heat generation terms*, Engineering Analysis with Boundary Elements, **51**, 191–198, 2015.
12. P. OYARZÚN, F.S. LOUREIRO, J.A.M. CARRER, W.J. MANSUR, *A time-stepping scheme based on numerical Green's functions for the domain boundary element method: the ExGA-DBEM Newmark approach*, Engineering Analysis with Boundary Elements, **35**, 3, 533–542, 2011.

13. D.P.N. KONTONI, *Elastoplastic dynamic analysis by the DR-BEM in modal co-ordinates*, WIT Transactions on Modelling and Simulation, WIT Press, **3**, 191–202, 1993.
14. M. KÖGL, L. GAUL, *A boundary element method for transient piezoelectric analysis*, Engineering Analysis with Boundary Elements, **24**, 7–8, 591–598, 2000.
15. C.-C. CHIEN, Y.-H. CHEN, C.-C. CHUANG, *Dual reciprocity BEM analysis of 2D transient elastodynamic problems by time-discontinuous Galerkin FEM*, Engineering Analysis with Boundary Elements, **27**, 6, 611–624, 2003.
16. E.L. ALBUQUERQUE, P. SOLLERO, M.H. ALIABADI, *Dual boundary element method for anisotropic dynamic fracture mechanics*, International Journal for Numerical Methods in Engineering, **59**, 9, 1187–1205, 2004.
17. X. LU, W.-L. WU, *A subregion DRBEM formulation for the dynamic analysis of two-dimensional cracks*, Mathematical and Computer Modelling, **43**, 1–2, 76–88, 2006.
18. J. USECHE, E.L. ALBUQUERQUE, *Dynamic analysis of shear deformable plates using the dual reciprocity method*, Engineering Analysis with Boundary Elements, **36**, 5, 627–632, 2012.
19. J. USECHE, E.L. ALBUQUERQUE, *Transient dynamic analysis of shear deformable shallow shells using the boundary element method*, Engineering Structures, **87**, 1–7, 2015.
20. P.H. WEN, M.H. ALIABADI, A. YOUNG, *A boundary element method for dynamic plate bending problems*, International Journal of Solids and Structures, **37**, 37, 5177–5188, 2000.
21. P.H. WEN, M.H. ALIABADI, *Boundary element frequency domain formulation for dynamic analysis of Mindlin plates*, International Journal for Numerical Methods in Engineering, **67**, 11, 1617–1640, 2006.
22. P.H. WEN, M.H. ALIABADI, *Laplace domain boundary element method for Winkler and Pasternak foundation thick plates*, in: Recent Developments in Boundary Element Methods, E.J. Sapountzakis [ed.], **43**, 323–333, 2010.
23. L. IGUMNOV, I. MARKOV, A. KONSTANTINOV, *Boundary element modeling of dynamic bending of a circular piezoelectric plate*, DYMAT 2018 International Conference, EPJ Web of Conferences, **183**, paper no: 01025, 2018.
24. E.J. SAPOUNTZAKIS, J.A. DOURAKOPOULOS, *Shear deformation effect in flexural-torsional vibrations of composite beams by boundary element method*, Journal of Vibration and Control, **16**, 12, 1763–1789, 2010.
25. E.J. SAPOUNTZAKIS, V.J. TSIPIRAS, A.K. ARGYRIDI, *Torsional vibration analysis of bars including secondary torsional shear deformation effect by the boundary element method*, Journal of Sound Vibration, **355**, 208–231, 2015.
26. K.M. RASMUSSEN, S.R.K. NIELSEN, P.H. KIRKEGAARD, *Boundary element method solution in the time domain for a moving time-dependent force*, Computers & Structures, **79**, 7, 691–701, 2001.
27. Y. QU, W. ZHANG, Z. PENG, G. MENG, *Time-domain structural acoustic analysis of composite plates subjected to moving dynamic loads*, Composite Structures, **208**, 574–584, 2019.
28. C.A. BREBBIA, D. NARDINI, *Dynamic analysis in solid mechanics by an alternative boundary element procedure*, Engineering Analysis with Boundary Elements, **24**, 4, 513–518, 2000.

29. S. HAMZEHEI JAVARAN, S. SHOJAEI, *The solution of elastostatic and dynamic problems using the boundary element method based on spherical Hankel element network*, International Journal for Numerical Methods in Engineering, **112**, 13, 2067–2086, 2017.
30. Y. FU, H. DU, S. ZHANG, *Functionally graded TiN/TiNi shape memory alloy films*, Materials Letters, **57**, 20, 2995–2999, 2003.
31. A. WITVROUW, A. MEHTA, *The use of functionally graded poly-SiGe layers for MEMS applications*, Materials Science Forum, **492–493**, 255–260, 2005.
32. H. HASSANIN, K. JIANG, *Net shape manufacturing of ceramic micro parts with tailored graded layers*, Journal of Micromechanics and Microengineering, **24**, 1, 015018, 2014.
33. F. YANG, A.C.M. CHONG, D.C.C. LAM, P. TONG, *Couple stress based strain gradient theory for elasticity*, International Journal of Solids and Structures, **39**, 10, 2731–2743, 2002.
34. H.M. MA, X.L. GAO, J.N. REDDY, *A microstructure-dependent Timoshenko beam model based on a modified couple stress theory*, Journal of the Mechanics and Physics of Solids, **56**, 12, 3379–3391, 2008.
35. M. ASGHARI, M.H. KAHROBAIYAN, M.T. AHMADIAN, *A nonlinear Timoshenko beam formulation based on the modified couple stress theory*, International Journal of Engineering Science, **48**, 12, 1749–1761, 2010.
36. M. ASGHARI, M. RAHAEIFARD, M.H. KAHROBAIYAN, M.T. AHMADIAN, *The modified couple stress functionally graded Timoshenko beam formulation*, Materials & Design, **32**, 3, 1435–1443, 2011.
37. M. ŞİMŞEK, T. KOCATÜRK, Ş.D. AKBAŞ, *Static bending of a functionally graded microscale Timoshenko beam based on the modified couple stress theory*, Composite Structures, **95**, 740–747, 2013.
38. M. ŞİMŞEK, J.N. REDDY, *Bending and vibration of functionally graded microbeams using a new higher order beam theory and the modified couple stress theory*, International Journal of Engineering Science, **64**, 37–53, 2013.
39. R. AGHAZADEH, E. CIGEROGLU, S. DAG, *Static and free vibration analyses of small-scale functionally graded beams possessing a variable length scale parameter using different beam theories*, European Journal of Mechanics – A/Solids, **46**, 1–11, 2014.
40. A. BABAEI, M.R.S. NOORANI, A. GHANBARI, *Temperature-dependent free vibration analysis of functionally graded micro-beams based on the modified couple stress theory*, Microsystem Technologies, **23**, 10, 4599–4610, 2017.
41. M.H. GHAYESH, M. AMABILI, H. FAROKHI, *Nonlinear forced vibrations of a microbeam based on the strain gradient elasticity theory*, International Journal of Engineering Science, **63**, 52–60, 2013.
42. R. VATANKHAH, M.H. KAHROBAIYAN, A. ALASTY, M.T. AHMADIAN, *Nonlinear forced vibration of strain gradient microbeams*, Applied Mathematical Modelling, **37**, 18–19, 8363–8382, 2013.
43. S. RAJASEKARAN, H.B. KHANIKI, *Size-dependent forced vibration of non-uniform bi-directional functionally graded beams embedded in variable elastic environment carrying a moving harmonic mass*, Applied Mathematical Modelling, **72**, 129–154, 2019.
44. D. DAS, *Nonlinear forced vibration analysis of higher order shear-deformable functionally graded microbeam resting on nonlinear elastic foundation based on modified couple*

stress theory, Proceedings of the Institution of Mechanical Engineers, Part L: Journal of Materials: Design and Applications, **233**, 9, 1773–1790, 2019.

45. G.G. SHENG, X. WANG, *Nonlinear forced vibration of size-dependent functionally graded microbeams with damping effects*, Applied Mathematical Modelling, **71**, 421–437, 2019.
46. J.C. HOUBOLT, *A recurrence matrix solution for the dynamic response of elastic aircraft*, Journal of the Aeronautical Sciences, **17**, 9, 540–550, 1950.
47. M. KERDJOUJ, F.M.L. AMIROUCHE, *Implementation of the boundary element method in the dynamics of flexible bodies*, International Journal for Numerical Methods in Engineering, **39**, 2, 321–354, 1996.
48. K.J. BATHE, E.L. WILSON, *Stability and accuracy analysis of direct integration methods*, Earthquake Engineering & Structural Dynamics, **1**, 3, 283–291, 1972.
49. D.E. JOHNSON, *A proof of the stability of the Houbolt method*, AIAA Journal, **4**, 8, 1450–1451, 1966.
50. T. MORI, K. TANAKA, *Average stress in matrix and average elastic energy of materials with misfitting inclusions*, Acta Metallurgica, **21**, 5, 571–574, 1973.
51. G.H. PAULINO, Z.-H. JIN, R.H. DODDS JR., *Failure of functionally graded materials*, in: Comprehensive Structural Integrity, I. Milne, R.O. Ritchie, B. Karihaloo [eds.], **2**, 607–644, 2003.
52. H.-S. SHEN, Z.-X. WANG, *Assessment of Voigt and Mori-Tanaka models for vibration analysis of functionally graded plates*, Composite Structures, **94**, 7, 2197–2208, 2012.
53. J.N. REDDY, Z.-Q. CHENG, *Frequency of functionally graded plates with three-dimensional asymptotic approach*, Journal of Engineering Mechanics, **129**, 8, 896–900, 2003.
54. A.J.M. FERREIRA, R.C. BATRA, C.M.C. ROQUE, L.F. QIAN, R.M.N. JORGE, *Natural frequencies of functionally graded plates by a meshless method*, Composite Structures, **75**, 1–4, 593–600, 2006.
55. C. ZHANG, Q. WANG, *Free vibration analysis of elastically restrained functionally graded curved beams based on the Mori-Tanaka scheme*, Mechanics of Advanced Materials and Structures, **26**, 21, 1821–1831, 2019.
56. J. SONG, Y. WEI, *A method to determine material length scale parameters in elastic strain gradient theory*, Journal of Applied Mechanics, Transactions of the ASME, **87**, Paper No: 031010, 2020.
57. R. ANSARI, R. GHOLAMI, S. SAHMANI, *Free vibration analysis of size-dependent functionally graded microbeams based on the strain gradient Timoshenko beam theory*, Composite Structures, **94**, 1, 221–228, 2011.
58. L. GARCIA, S. VILLAÇA, *Introduction to the theory of elasticity*, COPPE/UFRJ, 2000 [in Portuguese].

Received March 27, 2021; revised version June 20, 2021.

Published online August 13, 2021.